Ab Initio Interaction Potentials for Simulations of Dimethylnitramine Solutions in Supercritical Carbon Dioxide with Cosolvents

Robert Bukowski*,†,‡ and Krzysztof Szalewicz†

Department of Physics and Astronomy, University of Delaware, Newark, Delaware 19716, and Quantum Chemistry Laboratory, Department of Chemistry, University of Warsaw, Pasteura 1, 02-093, Warsaw, Poland

Cary F. Chabalowski

Army Research Laboratory, Aberdeen Proving Ground, Maryland 21005-5006

Received: April 14, 1999; In Final Form: July 2, 1999

Symmetry-adapted perturbation theory has been employed to calculate *ab initio* potential energy surfaces for complexes involved in the process of dissolving dimethylnitramine in supercritical carbon dioxide in the presence of acetonitrile or methyl alcohol as cosolvents. Site−site fits with correct asymptotic behavior have been developed for all potentials. The new potential energy surfaces can be used, along with the previously reported ones for carbon dioxide and carbon dioxide−acetonitrile dimers, in fully *ab initio* simulations of supercritical extraction processes. The physical interpretation of the features of the interaction potential energy surfaces resulting from the present approach challenges the established literature interpretations in terms of electrostatics only.

I. Introduction

Understanding the complicated physicochemical processes taking place in condensed phases has always been a challenge both from experimental and theoretical points of view. In recent years, with the advent of high-performance computers, the volume of theoretical contributions to these investigations has increased enormously. Simulation techniques such as molecular dynamics (MD) and Monte Carlo (MC) methods can provide a valuable insight into the structure and properties of bulk phases and into the mechanisms of processes occurring there.

A necessary ingredient in every simulation is the interaction potential governing the motion of the system, usually assumed as a sum over pair interactions between molecules. One way of obtaining a pair interaction potential is to assume a suitable functional form, most often a site−site formula, with a number of free parameters adjusted to reproduce some set of experimental data in MD/MC simulations. Although such empirically derived potentials may give reasonable predictions of properties other than the data used in the fit, they are known to often fail to do so. This indicates that empirical potentials fitted to bulk properties may differ significantly from true pair potentials. The main reason for the difficulty is that the former potentials implicitly take into account the many-body effects, which therefore cannot be separated and their impact on various properties cannot be assessed. An alternative method, free from the above deficiencies, is to calculate the interaction potentials from first principles, without any reference to experiments. Such an *ab initio* approach is much more difficult to implement since large basis sets and high theory level requirements must be met to obtain potentials of predictive quality. Moreover, strong anisotropy of the interaction between spatially extended systems can be accurately described only if a sufficiently dense grid in dimer coordinates is used in the calculations. Although these factors are still prohibitive for larger systems, with the recent progress in computer technology and *ab initio* methods of quantum chemistry the purely theoretical potentials are becoming more and more useful in bulk phase simulations of medium sized systems, i.e., for molecules consisting of a few atoms.

The *ab initio* methods of interaction energy calculations fall into two general categories. The first one is the supermolecular approach (see, e.g., ref 1 for a review) in which the interaction energy is obtained as the difference between the energy of the dimer (supermolecule) and the energies of the individual monomers. Although conceptually simple and easy to implement (the existing quantum chemistry codes can be used in the calculations without modification), the supermolecular method generates results in the form of single numbers, providing only a limited insight into the physical nature of the interaction. The second category contains computational methods based on the perturbative expansion of the energy in powers of the interaction operator. In particular, the method employed in the present work is the many-body implementation of the symmetry-adapted perturbation theory (SAPT).[2−4] One of the advantages of this approach over the supermolecular method is the interpretative value. The interaction energy is given as a sum of four fundamental components corresponding to different physical phenomena: electrostatic, induction, dispersion, and exchange forces. Each of these components is in turn expanded in terms of the intramonomer correlation operator. Further, since the SAPT approach does not suffer from the basis set superposition error (BSSE) problem, considerable freedom exists in the choice of basis sets used for different components of the interaction energy. In practice, saturated results can usually be obtained in basis sets smaller than the dimer-centered basis sets (DCBS) that must be used in the supermolecular approach to avoid BSSE. Finally, the direct correspondence of the perturbative scheme inherent in the SAPT method to the large-R expansion

* Corresponding author.
† University of Delaware.
‡ University of Warsaw.

10.1021/jp991212p CCC: $18.00
Published on Web 08/20/1999

TABLE 1: *Ab Initio* Pair Potentials Relevant for Simulations of DMNA in Supercritical CO_2 with CH_3OH or CH_3CN as Cosolvents[a]

A−B	ref	theory level	basis	grid	points
CO_2-CO_2	6	SAPT/LA	spdf+	30/−/45/30/−	220
CH_3CN-CO_2	7	SAPT/LA	spdf+	45/60/45/45/−	187
CH_3CN-CH_3CN	9	MBPT2	spd		336
	this work	SAPT/LA	spd+	60/60/60/60/60	373
CH_3OH-CH_3OH	this work	SAPT/LA	spd+	60/180/90/60/180	507
CH_3OH-CO_2	this work	SAPT/LA	spd+	30/90/90/30/−	920
$DMNA-CO_2$	this work	SAPT/LB	spd+	60/45/45/60/−	289
$DMNA-CH_3CN$	this work	SAPT/LB	spd+	60/60/90/60/40	504
$DMNA-CH_3OH$	this work	SAPT/LB	spd+	60/90/90/60/90	830
DMNA−DMNA	this work	SCF+$E_{disp}^{(20)}$	spd+	45/90/90/45/90	433

[a] Notation $D_{\beta_A}/D_{\gamma_A}/D_{\alpha_B}/D_{\beta_B}/D_{\gamma_B}$ indicates the intervals of different angular coordinates used to define basic angular grids. See sections II and IV for details on theory levels and grids, respectively.

of the interaction potential allows an accurate description of the asymptotic region without performing extensive long-range calculations.

One of the important problems investigated in recent years by both experimental and theoretical simulation methods is the process referred to as supercritical fluid extraction (SFE), which involves dissolving various chemical species in liquid carbon dioxide under the supercritical conditions. In these conditions, properties of the solvent may be varied over a wide range to maximize solubility. In some cases the solubility may be increased by augmenting the solvent−solute mixture with additional substances referred to as cosolvents. The SFE technique has been excessively investigated in relation to an industrially and environmentally important problem of recycling of aging propellants and explosives containing nitramines, such as cyclotrimethylenetrinitramine (RDX) and cyclotetramethylenetetranitramine (HMX), as the main components. The experimental work shows (see the literature review in ref 5) that these compounds can be effectively recovered in the supercritical extraction process with carbon dioxide as a solvent. Small solubility of nitramines in pure supercritical CO_2 can be enhanced by admixture of cosolvents, such as acetonitrile (CH_3CN) or methyl alcohol (CH_3OH).

Investigations of solvent−solute binding and the role of cosolvents are crucial for understanding the whole dissolution process and designing optimal conditions to perform it. The goal of the present work is to address this problem from theoretical point of view by generating a set of *ab initio* SAPT pair potentials relevant for simulations of the supercritical extraction process with the cosolvents mentioned above. Since the RDX or HMX molecules are still too large to be effectively treated by sufficiently accurate *ab initio* methods, we have chosen dimethylnitramine (DMNA) as the solute. Although the DMNA molecule is much smaller than RDX (in fact, RDX may be thought of as a "trimer" formed by three DMNA molecules arranged in a ring), it is expected to have all the characteristic features of the latter as far as the interactions with solvent and cosolvent molecules are concerned.

The complete description of this problem requires nine potential energy surfaces. The current status of the *ab initio* calculations for these surfaces is summarized schematically in Table 1. Two of the required interaction potentials, namely the CO_2-CO_2 potential[6] and the CH_3CN-CO_2 potential,[7] have been calculated previously using the SAPT approach. We refer to refs 6 and 7 for reviews of literature potentials for those systems. For the $(CH_3CN)_2$ complex, several empirical site−site potentials have been developed and applied in bulk phase and clusters simulations. These potentials are based either on a three-site model,[8,10] in which the methyl group is represented by a single site, or on a six-site representation of the monomer,[11,12] with sites located on each of the atoms. The interactions between each pair of sites are described by the electrostatic and Lennard-Jones terms. Recently, Cabaleiro-Lago and Ríos reported the first purely *ab initio* potential for $(CH_3CN)_2$.[9] The interaction energies, calculated at about 300 dimer geometries using the supermolecular MP2/6-311+G* approach, were fitted to a six-site exp + R^{-6} formula augmented with Coulomb interactions between point charges. In the present work, we propose an alternative *ab initio* potential, based of the SAPT theory of intermolecular interactions.

A number of empirical potentials have been developed for the $(CH_3OH)_2$ dimer by comparing the results of bulk phase simulations with experimental data. Perhaps the most popular of them are the "optimized potential for liquid simulation" (OPLS) of Jorgensen,[13] the so-called PHH3 potential of Pálinkás et al.,[14] and the "empirical potential based on electrons and nuclei" (EPEN/2) of Snir et al.[15] The OPLS and PHH3 potentials are based on a three-site Lennard-Jones + electrostatics site−site interactions (methyl group is treated as one site), with additional Morse-type hydrogen bond terms in the case of the PHH3 function. In the EPEN/2 model a monomer is represented as a number of charges representing nuclei, chemical bonds, and lone electron pairs. The interaction energy between two monomers is then calculated as the sum of Coulomb terms between all charged sites, and the exp + R^{-6}-type terms between the sites representing the electrons. The same functional form is assumed in the "quantum mechanical potential based on electrons and nuclei" (QPEN) model,[16] in which the parameters have been fitted to the *ab initio* data for several prototype molecules. Interaction potentials for other systems (including CH_3OH dimer) are then constructed by assuming transferability of the fit parameters. Although the QPEN model may be regarded as an early *ab initio* attempt to calculate the interaction energy in the CH_3OH dimer, the SAPT potential presented in this work is the first complete fully *ab initio* calculation for this system.

To our knowledge, no empirical or *ab initio* potentials have previously been reported for complexes involving the DMNA molecule. The $DMNA-CO_2$, $DMNA-CH_3CN$, $DMNA-CH_3OH$, and $(DMNA)_2$ potential energy surfaces proposed in this work represent the first description of interactions in such complexes.

The plan of the paper is as follows: In section II the highlights of the SAPT approach are given, followed by a description of a novel fitting strategy in section III. Section IV deals with computational details common to all the systems considered, while discussion of the specific features of the seven potential energy surfaces is given in section V. In section VI we discuss the accuracy of our potentials and compare the calculated values of the second virial coefficient to the available experimental data. Finally, in section VII, summary of the results and conclusions are presented.

II. Outline of the Symmetry-Adapted Perturbation Theory

A detailed account of the many-body SAPT approach has been given in refs 2−4 and 17−19; a summary will be presented here. The foundation of the method is a double perturbation theory based on the following decomposition of the total clamped-nuclei Hamiltonian H_{AB} of the dimer:

$$H_{AB} = F_A + F_B + V + W \tag{1}$$

where F_X is the Fock operator of monomer X, V is the interaction potential, W is the intramonomer correlation operator, and the last two operators are treated as perturbations. The Rayleigh−Schrödinger double perturbation expansion based on the decomposition (1) is known as polarization theory. To properly account for the exchange of electrons between the subsystems, in each order in V the wave function is adapted to the appropriate permutational symmetry which provides exchange energy components. As a result, the interaction energy E_{int} of closed-shell monomers A and B with centers of mass separated by vector $\boldsymbol{R}$ and with angular configurations given by Ω is calculated directly as a sum of *polarization* corrections $E_{pol}^{(nm)}$ and *exchange* corrections $E_{exch}^{(nm)}$

$$E_{int}(\boldsymbol{R},\Omega) = \sum_{n=1}^{\infty}\sum_{m=0}^{\infty}(E_{pol}^{(nm)} + E_{exch}^{(nm)}) \tag{2}$$

where the superscripts n and m denote the order in the V and W operators, respectively. Summing up over the intramonomer correlation index, we obtain the nth-order polarization and exchange corrections

$$E_{pol}^{(n)} = \sum_{m=0}^{\infty} E_{pol}^{(nm)}, \quad E_{exch}^{(n)} = \sum_{m=0}^{\infty} E_{exch}^{(nm)} \tag{3}$$

One of the advantages of the method is its interpretative value: each of the perturbative corrections, at least in low orders, has a clear physical meaning. For example, the first-order polarization correction is equal to the classical electrostatic interaction between two unperturbed charge distributions

$$E_{elst} \equiv E_{pol}^{(1)} \tag{4}$$

The second-order polarization corrections can be split into the *induction* and *dispersion* components

$$E_{pol}^{(2)} = E_{ind}^{(2)} + E_{disp}^{(2)} \tag{5}$$

and as a consequence

$$E_{exch}^{(2)} = E_{exch-ind}^{(2)} + E_{exch-disp}^{(2)} \tag{6}$$

While the induction energy represents asymptotically the classical interaction between permanent and induced multipole moments, the dispersion and exchange energies are purely quantum effects. The dispersion energy arising from the intermonomer electron correlation can be roughly described as an interaction between instantaneous multipole moments on the monomers. For dimers consisting of nonpolar molecular species it is the primary attractive effect. The sum of the exchange corrections represents the so-called exchange repulsion E_{exch} resulting from resonance tunneling of electrons between the subsystems.

In practice it is sufficient to truncate the expansion in powers of V at the second order. The intramonomer perturbative series can be truncated at $m = 0$, $m = 2$, or $m = 3$, depending on the correction, although more accurate intramonomer correlation treatments, like coupled cluster singles and doubles (CCSD), are also possible. In particular, one can easily include the effect of distortion (response) of the orbitals of one monomer in the presence of the other. This leads to the "response" corrections, e.g., $E_{elst,resp}^{(12)}$ or $E_{ind,resp}^{(20)}$.

In practical applications of the SAPT method the interaction energy can be expressed as a sum of four fundamental components: electrostatic, induction, dispersion, and exchange energies

$$E_{int}(\boldsymbol{R},\Omega) = E_{elst} + E_{ind} + E_{disp} + E_{exch} \tag{7}$$

with the following approximations:

$$E_{elst} = E_{elst}^{(10)} + E_{elst,resp}^{(12)} + E_{elst,resp}^{(13)} \tag{8}$$

$$E_{ind} = E_{ind,resp}^{(20)} + {}^{t}E_{ind}^{(22)} \tag{9}$$

$$E_{disp} = E_{disp}^{(20)} + E_{disp}^{(21)} + E_{disp}^{(22)} \tag{10}$$

$$E_{exch} = E_{exch}^{(10)} + E_{exch}^{(11)} + E_{exch}^{(12)} + E_{exch-ind,resp}^{(20)} + {}^{t}E_{exch-ind}^{(22)} + E_{exch-disp}^{(20)} + \delta_{HF} \tag{11}$$

where ${}^{t}E_{ind}^{(22)}$ denotes the portion of $E_{ind}^{(22)}$ not included in $E_{ind,resp}^{(20)}$ and the quantity δ_{HF} is the difference between the supermolecular Hartree−Fock interaction energy and $E_{elst}^{(10)} + E_{exch}^{(10)} + E_{ind,resp}^{(20)} + E_{exch-ind,resp}^{(20)}$. Although δ_{HF} is not of purely exchange character, it is usually very small and can be included in E_{exch} for convenience. The level of SAPT defined by eqs 8−11 will be referred to as the LA level. The intramonomer correlation corrections are computationally demanding, e.g., the correction $E_{disp}^{(22)}$ involves triple excitations on each monomer and scales comparably to the supermolecular many-body perturbation theory at fourth-order (MBPT4) calculation. Therefore, for larger systems, or where very high accuracy is not a crucial issue, it is more feasible to lower the intramonomer correlation level of the calculated interaction energy. The most straightforward simplification consists of removing from formulas (8)−(11) all terms with $m > 0$. Expressions for the fundamental interaction energy components become then

$$E_{elst} = E_{elst}^{(10)} \tag{12}$$

$$E_{ind} = E_{ind,resp}^{(20)} \tag{13}$$

$$E_{disp} = E_{disp}^{(20)} \tag{14}$$

$$E_{exch} = E_{exch}^{(10)} + E_{exch-ind,resp}^{(20)} + E_{exch-disp}^{(20)} + \delta_{HF} \tag{15}$$

Equations 12−15 define an approximate level of SAPT which will be referred to as LB.

It is worthwhile to notice that the inclusion of the term δ_{HF} in expressions 11 and 15 allows one to interpret the interaction energy resulting from the SAPT method as a sum of the supermolecular SCF component and the correlation component

$$E_{int} = E_{int}^{HF} + E_{int}^{CORR} \tag{16}$$

where E_{int}^{CORR} consists of all terms with $m > 0$ appearing on the rhs of eqs 8−11 plus $E_{disp}^{(20)}$ and $E_{exch-disp}^{(20)}$. In the simplified version of the method E_{int}^{CORR} is represented only by the two latter terms.

The perturbative nature of SAPT approach is directly related to the asymptotic expansion of the interaction energy which can be obtained by replacing the operator V by its multipole expansion. Then in the large-R region the interaction energy can be well approximated by

$$E_{\text{int}} = \sum_n \frac{C_n(\hat{\boldsymbol{R}},\Omega)}{R^n} \tag{17}$$

with coefficients $C_n(\hat{\boldsymbol{R}},\Omega)$ expanded in terms of the complete set of angular functions

$$C_n(\hat{\boldsymbol{R}},\Omega) = \sum_{L_A,K_A,L_B,K_B,L} C_n^{\{\Lambda\}} A_{\{\Lambda\}}(\hat{\boldsymbol{R}},\Omega) \tag{18}$$

where Λ stands for a set of integers L_A, K_A, L_B, K_B, L, and

$$A_{\{\Lambda\}}(\hat{\boldsymbol{R}},\Omega) = (-1)^{L_A+L_B+L} \sum_{M_A=-L_A}^{L_A} \sum_{M_B=-L_B}^{L_A} \sum_{M=-L}^{L} \begin{pmatrix} L_A & L_B & L \\ M_A & M_B & M \end{pmatrix} \times D^{L_A}_{M_A,K_A}(\omega_A)^* D^{L_B}_{M_B,K_B}(\omega_B)^* C_{LM}(\hat{\boldsymbol{R}})$$

In the above equation, $\omega = (\omega_A, \omega_B)$, where ω_A and ω_B are the sets of Euler angles describing the orientation of monomers A and B, respectively, $\hat{\boldsymbol{R}}$ is the orientation of the vector pointing from A to B, $D^L_{M,K}(\omega)$ are the standard rotation matrixes, and $C_{LM}(\hat{\boldsymbol{R}})$ is a spherical harmonic in Racah normalization.[20] Up to the second order in V we have

$$C_n^{\{\Lambda\}} = C_{n,\text{elst}}^{\{\Lambda\}} + C_{n,\text{ind}}^{\{\Lambda\}} + C_{n,\text{disp}}^{\{\Lambda\}} \tag{19}$$

The van der Waals constants on the rhs of this equation are given in terms of only the monomer properties, namely the multipole moments and dynamic polarizabilities.[21,22] These properties can be computed *ab initio* using the POLCOR program of Wormer and Hettema[23] at the intramonomer correlation levels consistent with the levels of short-range SAPT calculations. In this way, an arbitrary number of large-R configurations can be accounted for by only a single-point calculation of the van der Waals constants.

III. Fitting Strategy

The interaction energies calculated on a grid of points can be fitted using various analytic representations. Expansions in terms of angular functions of eq 19 are especially useful here, since they may be tailored directly to the asymptotic expansion, eq 17, assuring the proper asymptotic behavior of the fit. This strategy proved very effective for smaller systems, where very high accuracy of the fit was required.[6,24] However, for complexes composed of larger molecules, convergence of the angular expansion is expected to be much slower. Moreover, computational cost of evaluating the angular functions seriously diminishes their usefulness for the bulk phase simulations. Therefore, in the present work we decided to employ the site−site fitting scheme modified to improve the description of the large-R asymptotic region of the potential energy surface.

The analytic representation of the interaction energy is assumed in the form

$$E_{\text{int}} = \sum_{a\in A}\sum_{b\in B}\left[e^{\alpha_{ab}-\beta_{ab}r_{ab}}\left(\frac{\kappa}{r_{ab}} + A_{ab}\right) + f_1(\delta_1^{ab} r_{ab})\frac{q_a q_b}{r_{ab}} + \sum_{n=6,8,\ldots} f_n(\delta_n^{ab} r_{ab})\frac{C_n^{ab}}{r^n_{ab}}\right] \tag{20}$$

where κ = Å × kcal/mol and sites a and b are located mostly on atoms, although for CO_2 and CH_3OH several off-atom centers have also been defined. The Coulomb terms, proportional to the products of site charges q_a, q_b, are responsible for description of the electrostatic component of the interaction energy, while the C_n^{ab}/r_{ab}^n terms mimic the induction and dispersion components. The Tang−Toennies[25] damping function

$$f_n(x) = 1 - e^{-x}\sum_{k=0}^{n}\frac{x^k}{k!} \tag{21}$$

attenuates the asymptotic terms at small distances, where they become unphysically large. It should be noted that eq 20 formally allows to define site pairs that experience only specific types on interactions. For example, by setting A_{ab} and C_n^{ab} equal to zero and $\beta_{ab} \rightarrow \infty$ we can "turn off" the contributions of the pair a,b to exponential repulsion or dispersion energies, and make these sites interact only via the Coulomb forces.

The parameters of the fit (α_{ab}, β_{ab}, A_{ab}, q_a, q_b, C_n^{ab}, δ_n^{ab}) were determined in three steps. First, the charges q_a and q_b located on and off the atoms were least-squares fitted to the multipole moments of the monomers calculated *ab initio* in the monomer part of the basis set and at the same correlation level as used in the finite-R calculations. In the second step, the coefficients C_n^{ab} were obtained by fitting the expression $\sum_n C_n^{ab}/r_{ab}^n$ to the sum of the *ab initio* dispersion and induction energies calculated on a grid of points with large R. In practice, such a set of points was obtained from the original grid by shifting the intermonomer distances by 3.0 Å. Rather than performing expensive SAPT calculations of induction and dispersion at these large-R geometries, we utilized the asymptotic expansion, eqs 17−19, with the coefficients $C_{n,\text{ind}}^{\{\Lambda\}}$ and $C_{n,\text{disp}}^{\{\Lambda\}}$ calculated from the *ab initio* multipole moments and polarizabilities of the monomers. In this way, the C_n^{ab} were effectively fitted to reproduce the true *ab initio* asymptotics of the dispersion and induction parts of the potential. In the last step of our procedure the nonlinear parameters α_{ab}, β_{ab}, δ_n^{ab}, and the linear parameters A_{ab}, were fitted to the total SAPT interaction energies. During this optimization the charges q_a and C_n^{ab} coefficients were held fixed, which assured the correct large-R behavior of the fit. In all our applications of this fitting scheme an energy-dependent weight was used in the last step. Points with energies $E < 3$ kcal/mol were assigned weight w equal to 1, while for the remaining points $w = 1/(0.1E^2)$ was chosen.

It should be pointed out that the strategy we use to model electrostatic component of the interaction differs from the widely used method of fitting site charges to the electrostatic potential of a molecule. We rejected this method since it cannot reproduce correctly the higher-order multipoles. The reason is that in order to avoid a contamination by charge-overlap effects, which cannot be reproduced by the point charges, the fit points have to be chosen reasonably far from the center of the molecule and at these distances the contribution of higher multipoles is small. In addition, this method has nonuniqueness problems connected with arbitrariness in the choice of grid points. Our fitting strategy is free from these drawbacks. At the same time, the point charge representation of the electrostatic interaction is much simpler than models based on distributed or central multipoles. This simplicity makes it easier to port our fits to MC and MD programs.

IV. Computational Details

A. Monomer Geometries. Due to the difference in time scales of the intra- and intermolecular motions, it is reasonable to treat monomers as rigid molecules in their vibrational ground

TABLE 2: Geometry (in Å) and Site Charges (in au) of the Monomers Considered

site	*x*	*y*	*z*	q^a	q^b
DMNA[c]					
C_1	1.310 086	0.0	−1.310 271	0.202 997 412 38	
C_1	−1.310 086	0.0	−1.310 271	0.202 997 412 38	
N_1	0.0	0.0	−0.665 628	0.729 175 593 22	
N_2	0.0	0.0	0.716 671	−0.237 633 431 93	
O_1	1.110 211	0.0	1.229 661	−0.178 728 218 62	
O_1	−1.110 211	0.0	1.229 661	−0.178 728 218 62	
H_1	2.001 814	0.0	−0.428 395	−0.074 941 330 59	
H_2	1.267 695	−0.939 273	−1.920 321	−0.097 549 471 90	
H_2	1.267 695	0.939 273	−1.920 321	−0.097 549 471 90	
H_1	−2.001 814	0.0	−0.428 395	−0.074 941 330 59	
H_2	−1.267 695	0.939 273	−1.920 321	−0.097 549 471 90	
H_2	−1.267 695	−0.939 273	−1.920 321	−0.097 549 471 90	
CH_3CN[d]					
C_1	0.0	0.0	−0.168 927	0.483 438 672 63	0.472 786 304 71
C_2	0.0	0.0	1.309 019	−0.739 542 803 90	−0.667 115 933 22
N	0.0	0.0	−1.339 824	−0.484 537 626 20	−0.464 386 744 06
H	1.035 345	0.0	1.680 367	0.246 880 585 85	0.219 572 124 19
H	−0.517 673	0.896 635	1.680 367	0.246 880 585 85	0.219 572 124 19
H	−0.517 673	−0.896 635	1.680 367	0.246 880 585 85	0.219 572 124 19
CH_3OH[e]					
C	0.015 484	0.0	−0.730 324	−14.987 986 661 867	−14.187 773 403 691
O	−0.065 695	0.0	0.691 960	−0.223 828 857 208	−0.235 424 298 338
H_1	−1.010 213	0.0	−1.109 671	0.121 279 532 527	0.119 578 875 381
H_2	0.528 333	−0.888 280	−1.109 671	−0.043 739 256 713	−0.036 898 265 024
H_2	0.528 333	−0.888 280	−1.109 671	−0.043 739 256 713	−0.036 898 265 024
H_3	0.811 804	0.0	1.042 946	0.542 026 606 082	0.535 038 325 207
D_1	−0.057 574	0.0	0.549 730	−0.832 929 986 959	−0.775 737 427 645
D_2	0.014 574	0.0	−0.714 389	15.468 917 880 859	14.618 114 459 140
D_3	−0.105 835	−0.317 506	0.793 766	0.0	0.0
D_3	−0.105 835	0.317 506	0.793 766	0.0	0.0
CO_2 in DMNA−CO_2 complex[f]					
C	0.0	0.0	0.0	2.992 984 150 128	
O	0.0	0.0	−1.162 046	0.253 714 932 178	
O	0.0	0.0	1.162 046	0.253 714 932 178	
D_1	0.0	0.0	−0.687 930	−1.750 207 007 242	
D_1	0.0	0.0	0.687 930	−1.750 207 007 242	
D_2	0.0	0.0	−0.581 023	0.0	
D_2	0.0	0.0	0.581 023	0.0	
CO_2 in CH_3OH−CO_2 complex[g]					
C	0.0	0.0	0.0		6.856 857 511 739
O	0.0	0.0	−1.162 046		−0.048 414 269 147
O	0.0	0.0	1.162 046		−0.048 414 269 147
D_1	0.0	0.0	−0.317 506		−3.380 014 486 722
D_1	0.0	0.0	0.317 506		−3.380 014 486 722
D_2	0.0	0.0	−0.581 023		0.0
D_2	0.0	0.0	0.581 023		0.0

[a] Charges used in fits for complexes involving DMNA; fitted to the SCF multipole moments calculated in appropriate basis sets. [b] Charges used for complexes not involving DMNA; fitted to relaxed MBPT2 or MBPT3 (CH_3CN) multipole moments calculated in appropriate basis sets. [c] Reference 29, H-C-H angles optimized in this work at the MBPT2 level. [d] Reference 7, *ab initio* optimization at the QCISD level. [e] Reference 28, rotational spectra. [f] Reference 27, deduced from rotational constant B_0. Charges and dummy charged sites positions fitted to multipole moments calculated in the 3s2p1d basis set at the SCF level. [g] Reference 27, deduced from rotational constant B_0. Charges and dummy charged sites positions fitted to multipole moments calculated in the 4s2p1d basis set at the relaxed MBPT2 level.

states. In ref 26 it has been argued that potential energy surfaces generated using the vibrationally averaged monomer geometries should lead to the best results in theoretical predictions of infrared spectra. For larger systems, where accuracy of the potential is determined first of all by basis set size and the level of theory, the exact choice of monomer geometry is less important. It seems, however, that using geometries derived from experiment should be preferred over the ones optimized *ab initio*. This rule has been followed for all systems except CH_3CN, for which the QCISD-optimized geometry of ref 7 has been taken. The C−O distance in CO_2, equal to 1.162 047 Å, has been computed in ref 27 from the experimental rotational constant B_0 as an isotopically averaged value. Geometry of the CH_3OH molecule, also extracted from rotational spectra, has been taken from ref 28. The experimental DMNA configuration has been reported in ref 29 except for the H−C−H angles in methyl groups. These angles have been optimized by us at the MBPT2 level assuming the C_{2v} symmetry of the molecule[29] and keeping the other parameters at their experimental values.

Geometries of the monomers considered in this work are presented in Table 2 in the form of Cartesian coordinates, and in Figure 1. The fitted electric charges assigned to each site are also shown. Besides atoms, some molecules contain dummy sites denoted by D_n, serving as additional charges or exponential repulsion centers. Positions of these auxiliary sites have been roughly optimized during the fitting process.

B. Basis Sets. Since calculations of different potentials were originally started as separate projects, two different basis sets were used, depending on the system. For complexes involving DMNA and for $(CH_3CN)_2$ the isotropic part (3s2p) of the basis set was taken from cc-pVDZ basis of Dunning.[30] To this set we added d functions with exponents 0.281, 0.359, and 0.417

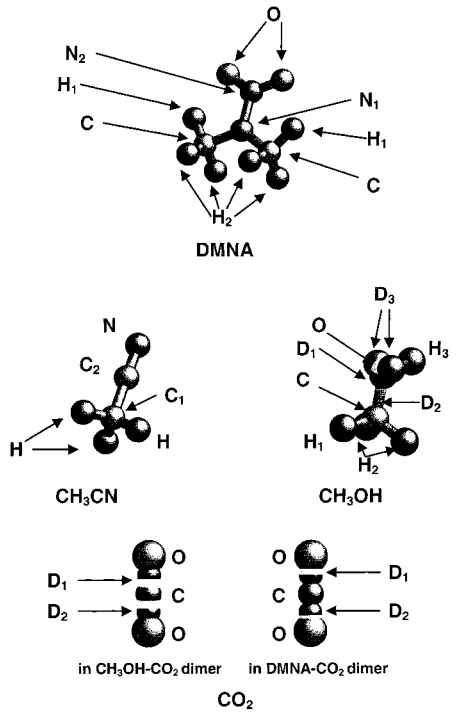

Figure 1. Monomers considered in this work and site labels.

for carbon, nitrogen, and oxygen, respectively, and a p function with the exponent 0.29 for hydrogen. These values of polarization exponents have been roughly optimized by us for the dispersion energy $E_{disp}^{(20)}$ in the preliminary calculations for the DMNA$-CO_2$ complex. To improve the description of the dispersion interaction, a 3s2p1d set of bond functions was placed midway between the centers of mass of the monomers, with s exponents equal to 0.553 063, 0.250 866, 0.117 111, p exponents equal to 0.392, 0.142, and the d exponent equal to 0.328. These bond functions have been taken from ref 31, where they have been used in the calculations for water dimer.

The same basis set has been used to describe the hydrogen atoms in the two remaining dimers, $(CH_3OH)_2$ and CH_3OH-CO_2. For the carbon and oxygen atoms in these systems we used a slightly different basis set obtained by contracting the isotropic parts of the 18s13p basis of Partridge[32] for carbon and oxygen to [4s2p]. The contracted primitives were 1−2 and 9−16 for the first orbital, 3−8 for the second, 9−16 for the third, and the second most diffuse function was left uncontracted. The contraction coefficients were taken from the 1s orbital for the first and second contracted functions and from the 2s for the third one. The p basis was obtained by contracting the first 10 exponents for the first contracted orbital, and the next two for the second one. The isotropic parts were augmented with dispersion energy optimized d functions with exponents 0.197 for carbon and 0.292 for oxygen. As bond functions for these dimers we used a subset of the bond functions set of ref 31, consisting of two s orbitals with exponents 0.553 063 and 0.250 866, and one p orbital with exponent equal to 0.392.

To speed up the calculations, the monomer-center-plus (MC^+ BS) basis set approach was employed for all systems except $(DMNA)_2$. The idea behind this methodology, introduced in ref 31, is to expand the orbitals of monomer A (B) in terms of all the basis functions centered on A, the bond functions, and only the isotropic part of the basis centered on B (A). As shown in ref 31, this approach allows us to match the full DCBS results using a much smaller number of basis functions.

C. Level of Theory. The choice of intramonomer correlation level of SAPT employed in the calculations was based on the size of the system, required level of accuracy, and the available computational resources. Combination of these factors determined two levels of theory: LA, given by eqs 8−11 and representing (except for some small correlation contributions to the first-order exchange energy) the highest available level of SAPT theory, and LB, defined by eqs 12−15. Calculations for complexes involving DMNA were performed at the lower level LB. It appears that for dimers of this size using this level with an spd basis augmented with bond functions provides sufficient accuracy at a reasonable computational cost.

An additional simplification had to be applied in the case of the largest complex considered in this work—the DMNA dimer. It turned out that the most cost-effective approach for this system consists of the supermolecular Hartree−Fock calculation followed by evaluation of the leading dispersion term, $E_{disp}^{(20)}$, both performed in the DCBS basis set. In this way the time-consuming two-electron integrals transformations and the SCF calculations can be limited to the necessary minimum, while still providing a reasonable estimate of the interaction energy. As a price for this simplification, the SCF interaction energy could not be split into physically meaningful components, and $E_{exch-disp}^{(20)}$ correction had to be neglected.

In the case of smaller dimers, consisting of the CO_2, CH_3OH, and CH_3CN molecules, it was possible to perform the calculations at the highest available level of theory, LA, asymptotically equivalent to the supermolecular MBPT4 approach. In spite of the relatively moderate size of the basis sets employed in this work, inclusion of the intramonomer correlation corrections to the interaction energy is still advantageous from the practical point of view, since these corrections tend to partially cancel the basis set incompleteness error. In particular, the usually negative $E_{disp}^{(22)}$ correction lowers the total dispersion energy, effectively reducing the basis set unsaturation effect on $E_{disp}^{(20)}$.

A more detailed discussion of the basis set quality and the accuracy of the applied theory levels will be postponed to section VI.

D. Dimer Geometries and Grids. The geometry of a dimer consisting of two rigid monomers can be described by the separation R of the centers of mass and the Euler angles of both monomers. The definition of Euler angles α, β, and γ employed in this work is that of Brink and Satchler.[20] It is convenient to assume that the vector pointing from the center of mass of monomer A to the center of mass of monomer B lies along the z axis. In this case, one angular variable can be easily eliminated, since the interaction potential depends on α_A and α_B only through the difference $\alpha_B - \alpha_A$. Thus, without the loss of generality the angle α_A can be set to zero, which reduces the dimensionality of the problem to six.

The coordinates described above have been used to define a grid of points for which the interaction energies were calculated. For each dimer a regular angular grid was constructed first by dividing the range of each angular coordinate into equal intervals and discarding the repetitious symmetry-equivalent configurations. The lengths of the intervals, shown for each system in Table 1, have been chosen in such a way that the resulting uniform grids provide a fairly good representation of the anisotropy of the potential energy surface with about 100 angular configurations. Some other characteristic configurations, if not covered by the regular grid, were also added. The resulting

angular grid was then repeated for different intermonomer separations R. The values of R were chosen initially to be 4.0, 5.0, and 6.0 Å and where necessary the short-range points were added in intervals of 0.5 Å until the repulsive wall of at least 10 kcal/mol was reached for each configuration. After the calculations for all points on the basic grids were completed, preliminary fits were performed from which approximate minima and other characteristic points on the surfaces were determined. The fits were then analyzed as functions of R for a large number (about 5000) of randomly selected angular configurations. This analysis allowed to pinpoint the configurations for which the fits behaved unphysically at short range, indicating the need for better representation of the repulsive wall. For all these configurations, as well as for the ones corresponding to the minima, the *ab initio* calculations were performed over the wide range of R covering the regions of the potential well and repulsive wall. These new points were then appended to the data files and used to generate the final fits. The total numbers of the calculated data points as well as the characteristics of the basic regular grids are presented in Table 1. Detailed results of the calculations (grid points and all the computed SAPT interaction energy components) as well as the parameters of the fits to the potential energy surfaces are presented in Tables S1−S14, supplied as Supporting Information.

E. Large-*R* Asymptotics. In order to assure the correct large-R asymptotic behavior of the fit, the site charges q_a and the site−site coefficients C_n^{ab} in eq 20 have to be chosen in such a way that the real *ab initio* asymptotics of the interaction energy is recovered. This is accomplished by fitting the site charges to the calculated multipole moments and the C_n^{ab} coefficients—to the sum of induction and dispersion energies calculated from the *ab initio* asymptotic expansion on a grid of long-range points, as described in section III. Such an approach requires the computation of multipole moments and dynamic polarizabilities, from which the dispersion and induction coefficients of eq 19 are obtained. When tailoring the asymptotic expansion to the finite-R SAPT interaction energies, some care must be taken of the appropriate intramonomer correlation level of the asymptotic constants, which should be consistent with the employed SAPT level. For example, the electrostatic energy in the large-R region is given in terms of products of multipole moments (see eq 37 of ref 4). To make this asymptotic expansion consistent with the SAPT level LA, defined by eqs 8−11, these products should undergo replacement schematically indicated by

$$Q^{\mathrm{A}}Q^{\mathrm{B}} \rightarrow Q^{\mathrm{A}}_{\mathrm{HF}}Q^{\mathrm{B}}_{\mathrm{HF}} + Q^{\mathrm{A}}_{\mathrm{HF}}\,(Q^{\mathrm{B}}_{\mathrm{MBPT2,resp}} + Q^{\mathrm{B}}_{\mathrm{MBPT3,resp}}) + (Q^{\mathrm{A}}_{\mathrm{MBPT2,resp}} + Q^{\mathrm{A}}_{\mathrm{MBPT3,resp}})\,Q^{\mathrm{B}}_{\mathrm{HF}} \quad (22)$$

where $Q^{\mathrm{X}}_{\mathrm{HF}}$ and $Q^{\mathrm{X}}_{\mathrm{MBPTn,resp}}$ are the multipole moments of system X calculated at the Hartree−Fock approximation and as field derivatives of the nth-order MBPT energies, respectively. Achieving strict compliance with eq 22 in the framework of our fitting strategy would be difficult, since the rhs of this equation is not a simple product of two quantities and hence there exists no well-defined correlation level of multipole moments to which the site charges should be fitted. Therefore, in the case of the LA level, where correlation corrections to electrostatics were taken into account, we decided to fit the site charges to the multipole moments approximated by $Q^{\mathrm{X}}_{\mathrm{HF}} + Q^{\mathrm{X}}_{\mathrm{MBPT2,resp}}$ (for the CH_3CN dimer the MBPT3,resp correction was also included). For systems treated at the LB level of SAPT, the rhs of the eq 22 reduces to the first term and it is clear that the site charges should be fitted to reproduce the multipole moments calculated at the Hartree−Fock level.

The induction asymptotic coefficients $C^{\{\Lambda\}}_{n,\mathrm{ind}}$ are given (see eq 38 of ref 4) in terms of products of multipole moments and static polarizabilities. For consistency with the SAPT calculations at LA level these products should undergo the following replacement:

$$\alpha^{\mathrm{A}}Q^{\mathrm{B}}Q^{\mathrm{B}'} \rightarrow \alpha^{\mathrm{A}}_{\mathrm{CHF}}Q^{\mathrm{B}}_{\mathrm{HF}}Q^{\mathrm{B}'}_{\mathrm{HF}} + {}^{\mathrm{t}}\alpha^{\mathrm{A}}_{\mathrm{MBPT2}}Q^{\mathrm{B}}_{\mathrm{HF}}Q^{\mathrm{B}'}_{\mathrm{HF}} + \alpha^{\mathrm{A}}_{\mathrm{UCHF}}Q^{\mathrm{B}}_{\mathrm{HF}}Q^{\mathrm{B}'}_{\mathrm{MBPT2}} + \alpha^{\mathrm{A}}_{\mathrm{UCHF}}Q^{\mathrm{B}}_{\mathrm{MBPT2}}Q^{\mathrm{B}'}_{\mathrm{HF}} \quad (23)$$

where Q^{X} and $Q^{\mathrm{X}'}$ denote two multipole moments (generally of different orders) of monomer X, $\alpha^{\mathrm{X}}_{\mathrm{CHF}}$ and $\alpha^{\mathrm{X}}_{\mathrm{UCHF}}$ are the coupled Hartree−Fock (CHF) and uncoupled Hartree−Fock (UCHF) polarizabilities, respectively, $Q^{\mathrm{X}}_{\mathrm{MBPT2}}$ is the second-order MBPT correction (without the orbital relaxation) to the multipole moment, and ${}^{\mathrm{t}}\alpha^{\mathrm{X}}_{\mathrm{MBPT2}}$ is the "true correlation"[33] second-order MBPT correction to the static multipole polarizability. Substitutions for products of dynamic polarizabilities in the expressions for the dispersion coefficients $C^{\{\Lambda\}}_{n,\mathrm{disp}}$ (see eq 39 of ref 4) are

$$\alpha^{\mathrm{A}}\alpha^{\mathrm{B}} \rightarrow \alpha^{\mathrm{A}}_{\mathrm{UCHF}}\alpha^{\mathrm{B}}_{\mathrm{UCHF}} + \alpha^{\mathrm{A}}_{\mathrm{UCHF}}\alpha^{\mathrm{B}}_{\mathrm{MBPT1}} + \alpha^{\mathrm{A}}_{\mathrm{MBPT1}}\alpha^{\mathrm{B}}_{\mathrm{UCHF}} + \alpha^{\mathrm{A}}_{\mathrm{MBPT1}}\alpha^{\mathrm{B}}_{\mathrm{MBPT1}} + \alpha^{\mathrm{A}}_{\mathrm{UCHF}}\alpha^{\mathrm{B}}_{\mathrm{MBPT2}} + \alpha^{\mathrm{A}}_{\mathrm{MBPT2}}\alpha^{\mathrm{B}}_{\mathrm{UCHF}} \quad (24)$$

where $\alpha^{\mathrm{X}}_{\mathrm{MBPT}n}$ is the nth-order MBPT correction (without orbital relaxation) to the dynamic polarizability of monomer X. All the correlation terms in eq 23 and 24 should be skipped if the LB level of SAPT is used, i.e., for all systems involving the DMNA molecule.

Calculations of all the needed multipole moments and polarizabilities as well as the subsequent evaluation of induction and dispersion coefficients $C^{\{\Lambda\}}_{n,\mathrm{ind}}$ and $C^{\{\Lambda\}}_{n,\mathrm{disp}}$ have been accomplished using the POLCOR suite of programs developed by Wormer and Hettema.[23] The multipole moments have been calculated in purely monomer parts of the basis sets through $L = 7$, and the asymptotic induction and dispersion coefficients through $n = 10$.

V. Results and Discussion

A. CH_3CN Dimer. Calculations of the interaction energy of this system have been performed for 373 configurations at the LA level of SAPT theory (eqs 8−11). The results have been summarized in Figures 2a,b, and in Tables 3, S1, and S2. The fit to the data points predicts existence of only one minimum M1, shown in Figure 2a along with three other interesting structures. The structure M1, experiencing an attractive effect of −5.65 kcal/mol (as obtained from the fit), corresponds to a slipped antiparallel configuration with the N atom of one molecule pointing to one of the methyl hydrogens of the other. Rotating one of the monomers by 60° around its axis weakens the interaction by 0.43 kcal/mol without significantly affecting the position of radial minimum. Very similar minimum geometries are predicted by other literature potentials.[9,11,13] The *ab initio* potential of Cabaleiro-Lago and Ríos[9] gives the intermonomer distance longer than ours by only 0.04 Å, and the β_{A} angle by 2° smaller. On the other hand, the minimum predicted by this potential is by 0.68 kcal/mol shallower than that of the SAPT potential. This significant difference results most likely from the fact that, due to the presence of bond functions in the basis set and due to the inclusion of the intramonomer correlation corrections, the dispersion interaction is saturated much better in our calculation than in the potential of ref 9.

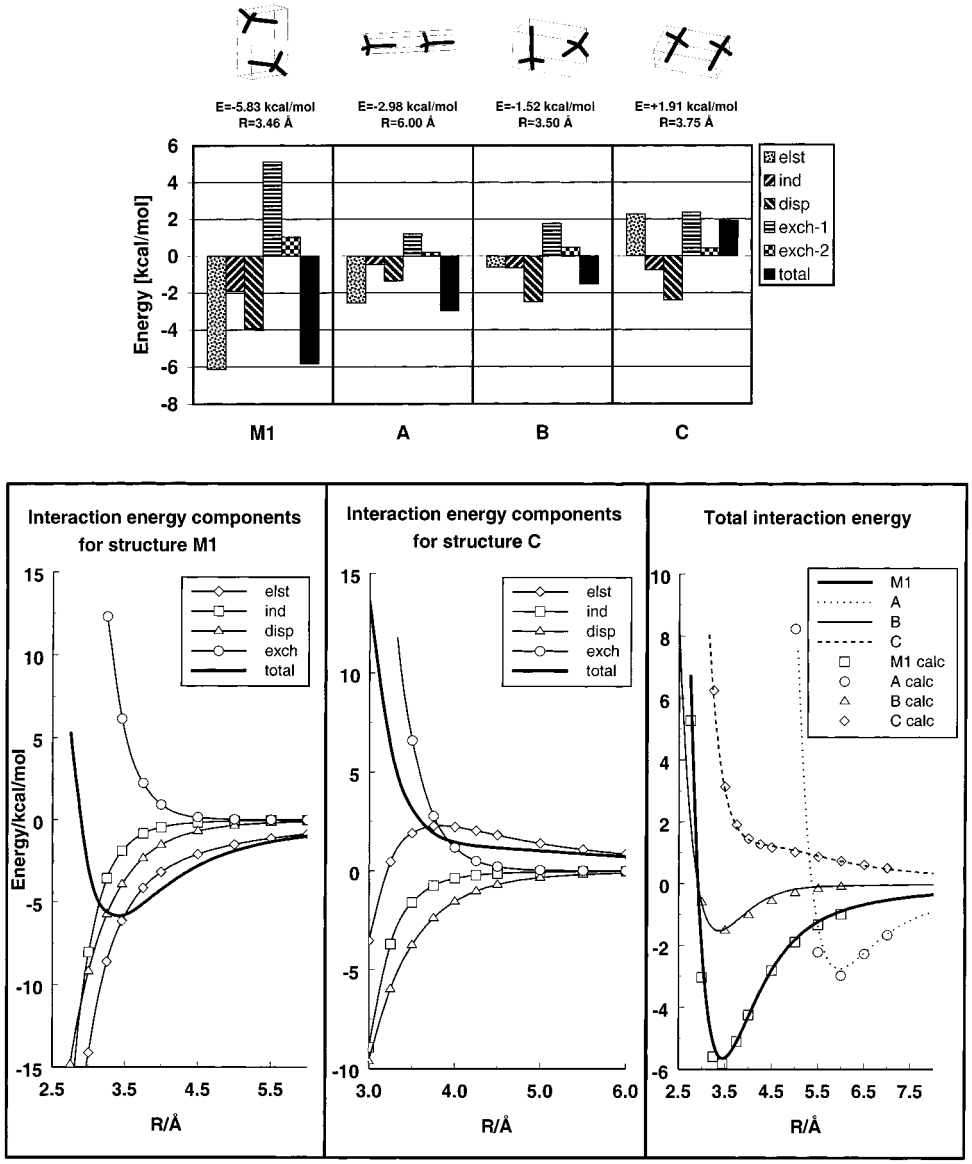

Figure 2. (a, top) Characteristic structures of the CH_3CN dimer and decomposition of the corresponding interaction energies. Labels exch-1 and exch-2 denote the first- and second-order contributions to the exchange energy, calculated as $E_{\mathrm{exch}}^{(10)} + E_{\mathrm{exch}}^{(11)} + E_{\mathrm{exch}}^{(12)}$ and $E_{\mathrm{exch-ind,resp}}^{(20)} + {}^{t}E_{\mathrm{exch-ind}}^{(22)} + E_{\mathrm{exch-disp}}^{(20)} + \delta_{HF}$, respectively. (b, bottom) Radial dependence of the interaction energy components for various structures of the CH_3CN dimer. Total interaction energy curves obtained from the fit. Single data points denoted by "calc" correspond to the actual calculated SAPT interaction energies.

The minimum structure predicted by the OPLS potential of Jorgensen[13] features a longer intermonomer distance (3.72 Å), the β_A angle equal to 74.8°, and substantially smaller interaction energy, amounting to −3.96 kcal/mol. The empirical six-site potential of Bohm et al.[11] gives the minimum with parameters closest to those predicted by the SAPT potential. With R value only by 0.02 Å shorter than the SAPT one, and β_A by 1.5° larger, the well depth turns out to be only 0.129 kcal/mol shallower than that of the SAPT potential.

As expected, electrostatics plays the dominant binding role in the structure M1, with somewhat smaller dispersion and significantly smaller induction. As can be seen from the radial plot of the interaction energy components in Figure 2b, this general pattern observed at the minimum is preserved for all intermonomer separations, although for larger R the magnitudes of dispersion and induction effects become quite close to each other. Very similar proportions of fundamental interaction energy components may be observed for configuration A, which is also bound due to the dipole−dipole interaction. It should be noted that although the dipoles arrangement in A is more favorable than in M1, the rapidly growing exchange effects destabilize the linear configuration at shorter distances. As a result the radial minimum in configuration A appears for R close to 6 Å and its depth is less than one-half of the depth of M1. Moreover, this radial minimum is just a saddle point when viewed from the perspective of the total potential energy surface.

The origin of bonding is different in configurations B and C, where dispersion energy turns out to be the main stabilizing factor. Due to the neutral dipoles orientation, the electrostatic interaction in B is very weak and comparable to induction. The repulsive arrangement of dipoles in configuration C results in a large positive electrostatic energy, which, together with the exchange repulsion, quenches the attractive contributions of dispersion and induction.

The total interaction energy for all configurations considered is shown as a function of R in the last plot of Figure 2b. The plot reflects high anisotropy of the system resulting from the large length of the monomers. While the radial minima for

TABLE 3: Parameters of the Minimum Structures of the Complexes Considered in This Work[a]

	R	β_A	γ_A	α_B	β_B	γ_B	E_{fit}	E_{calc}
$(CH_3CN)_2$								
M1	3.46	103.4	60.0	180.0	76.6	120.0	−5.65	−5.827
$(CH_3 OH)_2$								
M1	3.27	64.5	209.9	263.4	109.3	164.4	−4.87	−4.969
S	4.13	11.5	180.0	180.0	168.5	0.0	−4.06	−3.910
M2	3.66	96.0	0.0	180.0	84.0	180.0	−2.42	−2.136
CH_3OH-CO_2								
M1	3.17	55.2	329.1	163.7	103.1		−3.32	−3.526
M2	4.32	77.0	180.0	180.0	8.9		−1.92	−2.012
M3	4.12	171.7	180.0	180.0	94.7		−0.72	−0.541
$DMNA-CO_2$								
M1	3.47	70.8	61.3	141.9	124.4		−3.96	−3.893
M2	4.00	0.0	199.4	289.3	90.0		−3.18	−3.662
M3	5.62	180.0	0.0	0.0	0.0		−1.67	−1.552
$DMNA-CH_3CN$								
M1	3.22	75.4	90.0	0.0	67.7	240.0	−7.85	−7.850
M2	5.80	179.9	270.0	0.0	0.1	60.0	−3.82	−3.603
$DMNA-CH_3OH$								
M1	3.22	78.2	273.9	119.0	124.9	278.6	−5.85	−5.699
M2	4.35	10.2	0.0	180.0	92.9	0.0	−4.31	−4.638
$(DMNA)_2$								
M1	3.04	74.8	90.0	180.0	105.2	90.0	−10.74	−11.056
M2	4.27	100.2	90.0	180.0	155.1	180.0	−6.07	−5.934
M3	5.42	180.0	163.2	260.5	180.0	333.7	−5.08	−5.169
M4	4.68	166.8	0.0	180.0	113.9	270.0	−4.82	−4.855
M5	3.99	105.6	237.1	269.0	74.4	237.1	−4.35	−4.064

[a] E_{fit} is the energy obtained from the fit and E_{calc} is the corresponding *ab initio* result. Distances in Å, angles in degrees, and energies in kcal/mol.

configurations M1 and B occur around $R = 3.5$ Å, the minimum of A appears at a rather large distance of 6.0 Å. Notice that despite this large value of the centers of mass distance in the latter case, the separation of the closest atoms (H and N) is quite small, only 3.12 Å.

B. CH_3OH Dimer. Optimized parameters of the fit to the PES of this system obtained using 507 data points (Table S3) calculated at correlated theory level LA, eqs 8−11, are presented in Table S4. In order to reasonably reproduce the *ab initio* multipole moments of the CH_3OH molecule, it turned out to be necessary to introduce two additional charged sites, D_1 and D_2 (see Figure 1 and Table 2). These sites are assumed to contribute only to the electrostatic interactions and no exponential or induction/dispersion-type parameters are associated with them. Two other auxiliary sites of type D_3, simulating the lone electron pairs on the oxygen atom, are used to improve the description of exponentially decaying terms in the potential.

Two minimum structures M1 and M2 are shown in Figure 3a together with a low-energy flat second-order saddle point S and two other configurations A and B. As seen from the histograms of the interaction energy components, the M1 and S structures are bound mainly by large attractive electrostatic interactions with dispersion and induction being by a factor of 2 smaller. The radial plot of Figure 3b shows that the proportions of electrostatics, dispersion, and induction energies for the structure M1 are approximately constant for R larger than the minimum distance. Only after passing the minimum in the direction of the repulsive wall the proportions change as induction becomes more negative than dispersion. In the M1 configuration the orientation of molecular dipoles is attractive but not the most favorable and a large portion of strong electrostatic interaction comes from the quadrupole moments contribution. The directional character of the bond between the hydroxyl groups suggests a hydrogen bond character of the interaction. In fact, a very similar geometry and composition of the interaction energy are observed in the minimum configuration of the water dimer.[24] Although for geometrical reasons the possibility of forming a hydrogen bond in structure S must be excluded, the interaction energy ingredients have virtually the same proportions as for M1, with a dominant role of electrostatics. This large electrostatic component results mainly from the low-energy antiparallel orientation of dipoles, but also from the favorable arrangement of molecular quadrupoles.

To our knowledge, the minimum M2 has not been previously reported in the literature. To confirm the character of this structure we performed additional SAPT calculations for 42 geometries close to M2 located along the eigenvectors of the Hessian matrix. These calculations confirmed that the Hessian is indeed positive definite and thus M2 is a real minimum predicted by our method and not an artifact of the fit. The major portion of the binding effect in M2 results from very similar contributions of electrostatics and dispersion. A closer examination of the geometry reveals that the attractive electrostatic effect is mainly due to dipole−quadrupole and quadrupole−quadrupole interactions, since the antiparallel and almost linear alignment of dipoles results in a repulsive dipole−dipole contribution.

Structure A is an example of electrostatically repulsive configuration with unfavorable arrangement of dipoles. As seen in Figure 3b, the positive electrostatic component dominates the picture for R distances larger than 3.75 Å, exceeding both the fast-decaying exchange repulsion and the very small dispersion and induction effects. At smaller separations the latter become more significant and the electrostatic term becomes negative, but the growing exchange term does not allow a minimum to be generated and the curve remains repulsive for all R distances. A shallow minimum on the potential energy curve for configuration B results from the balance of the dispersion and first-order exchange effects. As suggested by Figure 3a which shows the energy decomposition at the radial minimum, the electrostatic, and especially induction components are negligible here.

Although electrostatic interaction is an important factor determining the stability of characteristic low-energy structures of the CH_3OH dimer, neither the energetics nor the geometry of these structures can be predicted from simple electrostatic

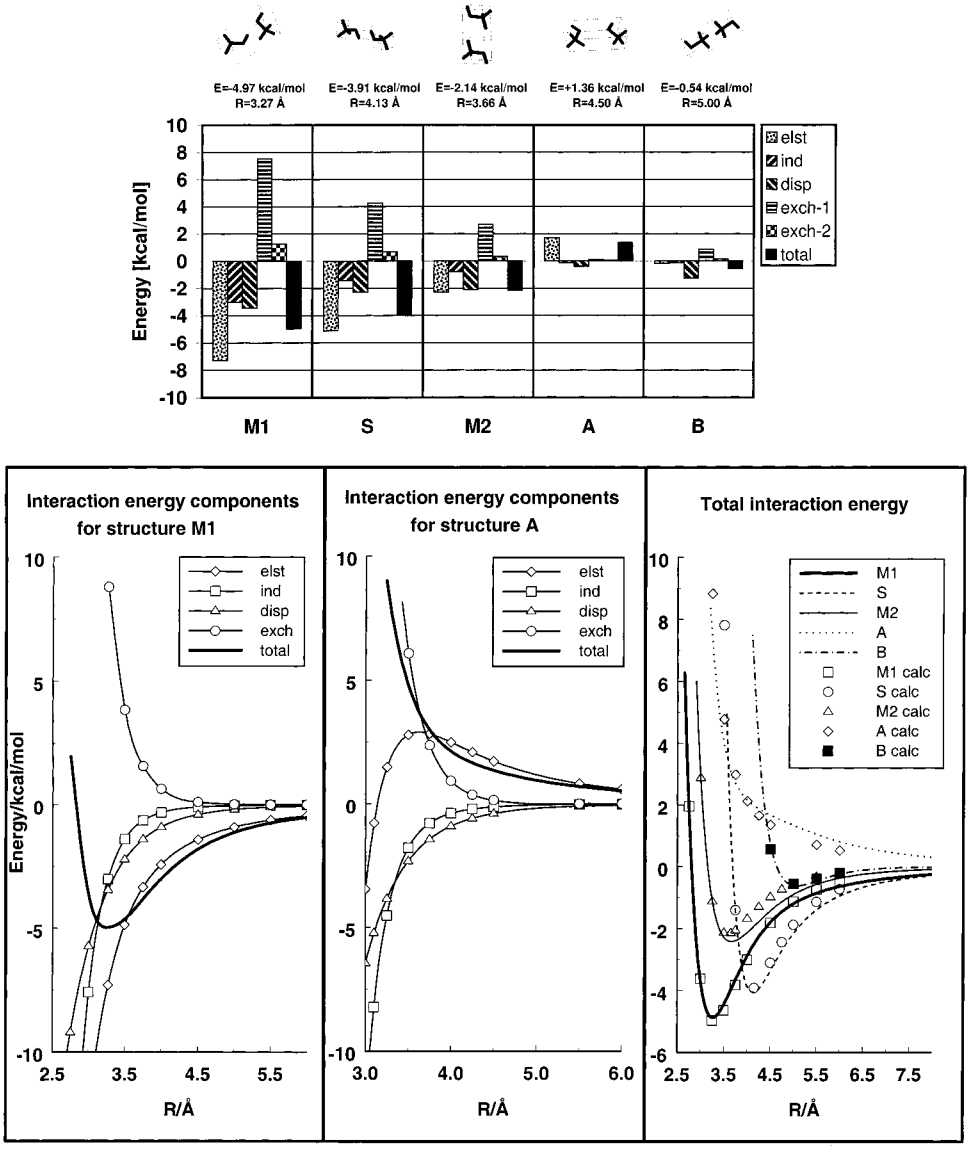

Figure 3. (a, top) Characteristic structures of the CH_3OH dimer and decomposition of the corresponding interaction energies. See caption for Figure 2a. (b, bottom) Radial dependence of the interaction energy components for various structures of the CH_3OH dimer. See caption for Figure 2b.

considerations. None of the structures M1, S, and M2 corresponds to the optimal (linear−parallel) dipoles orientation. While taking into account both dipole and quadrupole moments allows one to explain the dominant role of electrostatic interaction in these configurations, it is still not sufficient to determine the geometries even qualitatively.

It is interesting to compare the structural predictions derived from our potential to those of other potentials used in the literature to describe the CH_3OH dimer. Minimization of the OPLS[13] and QPEN[16] potentials detected only one minimum in each case. Geometries of these minima are similar to that of the global minimum M1, with slightly larger intermonomer distance (3.4 Å). On the other hand, the interaction energies of these structures, predicted by the OPLS and QPEN potentials to be equal to −6.88 and −9.71 kcal/mol, respectively, are significantly larger than the corresponding SAPT value of −4.87 kcal/mol obtained from our fit. In the case of the QPEN potential, this large discrepancy is most probably caused by the fact that the *ab initio* interaction energies, to which the parameters of the model were fitted, had not been corrected for the basis set superposition error (BSSE).

C. CH_3OH-CO_2 Complex. The fit for this system has been performed using 920 data points (Table S5) calculated using the LA level of the SAPT theory (eqs 8−11). The parameters of the fit are given in Table S6. Besides the interaction sites located on atoms, two additional types of sites have been introduced to better describe the CO_2 molecule. One of these types (D_1) carries a point charge, and the other one (D_2) serves as an exponential repulsion center. Structure and energetics of the three minimum structures M1−M3 and one additional configuration of the system are presented in Figures 4, a and b. The deepest minimum is the nonsymmetric M1 structure with the oxygen atom of CH_3OH pointing roughly toward the carbon atom of CO_2, and the hydroxyl hydrogen turned away from CO_2. In this configuration, corresponding to a favorable (although not optimal) dipole−quadrupole arrangement, the electrostatic interaction dominates the attractive part of the interaction energy. It is augmented with dispersion and induction energies very similar in magnitude and roughly a factor of 2 smaller than the electrostatics. Since the monomers approach each other relatively closely, the exchange components are also quite large. Figure 4b shows that the interaction energy composition in the

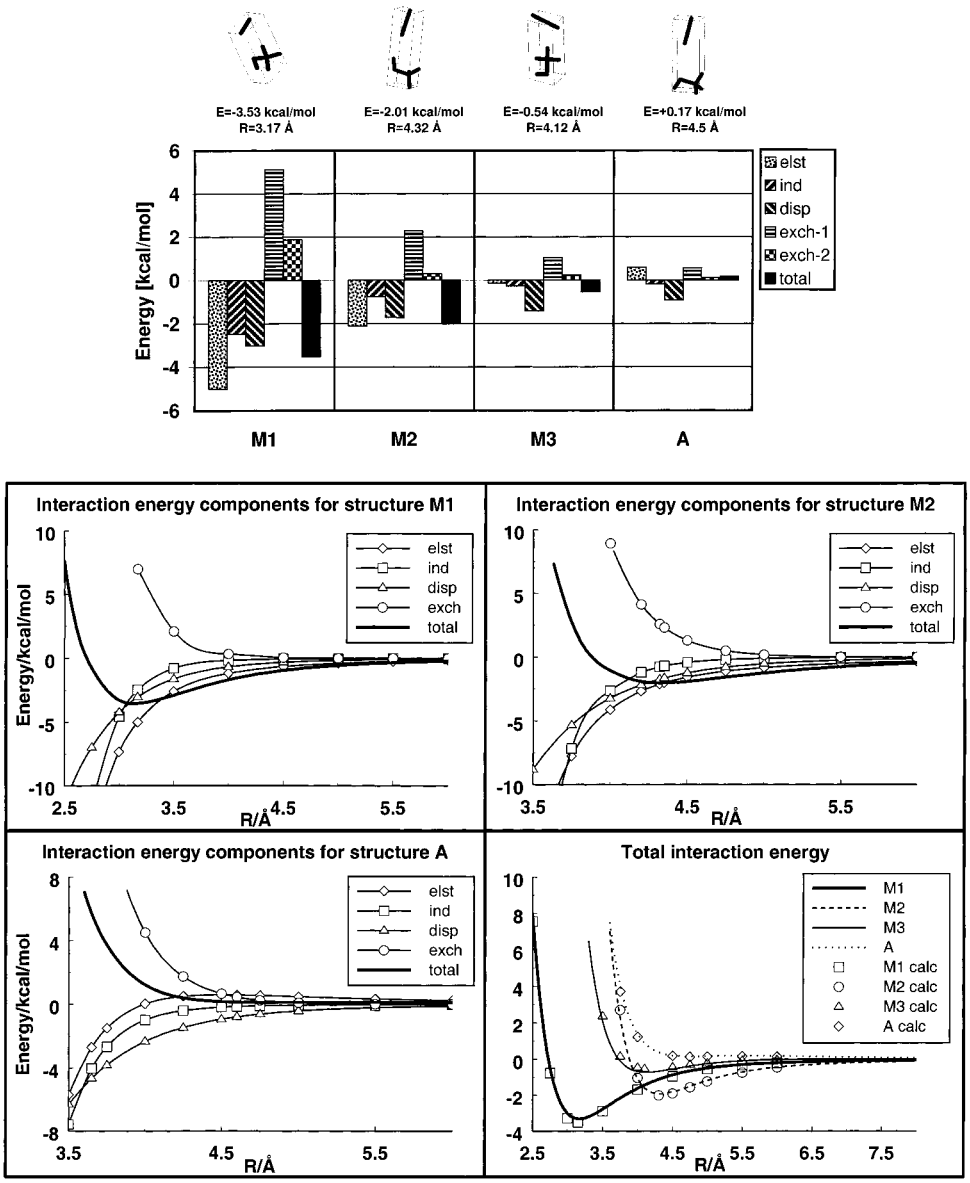

Figure 4. (a, top) Characteristic structures of the CH_3OH-CO_2 complex and decomposition of the corresponding interaction energies. See caption for Figure 2a. (b, bottom) Radial dependence of the interaction energy components for various structures of the CH_3OH-CO_2 complex. See caption for Figure 2b.

minimum M1 is, apart from the exponentially decaying exchange correction, constant for distances larger than the minimum distance. For distances only slightly to the left of the minimum, the induction energy becomes more negative than dispersion. For these distances, however, the growing exchange contribution starts to dominate the picture and generate the repulsive wall.

The geometry of the minimum M2 is very close to the one determined by the electrostatic energy restricted to the dipole−quadrupole and quadrupole-quadrupole interactions. Directional character of the bond with the hydroxyl hydrogen pointing toward the oxygen atom of CO_2 suggests a hydrogen bond-like stabilization of this structure. The decomposition of the interaction energy shows that this minimum represents one of the cases where electrostatics and dispersion play similar roles, while induction is much smaller than the former two components. Figure 4b shows that such a composition prevails throughout the entire range of *R* to the right of the minimum position. For distances penetrating into the repulsive wall the induction component grows in absolute value and eventually becomes more negative than either dispersion or electrostatics. Despite its hydrogen-bonded character, the M2 configuration is not the most stable one. It lies 1.5 kcal/mol above the global minimum M1, discussed earlier, which does not have the directional character of a hydrogen bond. Formation of hydrogen bonds cannot be therefore considered the main structure-determining factor.

For the weak minimum M3 the role of electrostatic interaction is much smaller than in previous structures. The small attractive effect results mainly from the balance between dispersion and first-order exchange energies.

Configuration A differs from the "hydrogen-bonded" M2 structure by rotation of the CH_3OH molecule around its *z* axis, which breaks the "hydrogen bond", and also changes the direction of the dipole moment of CH_3OH. As a result, the electrostatic energy becomes positive and cooperates with exchange to generate a completely repulsive interaction energy curve, shown in Figure 6b.

The last plot of Figure 4b presents the total interaction energies for all configurations considered as functions of *R*. As in the case of other complexes, the radial minima occur for very different values of *R*, indicating a substantial anisotropy of the

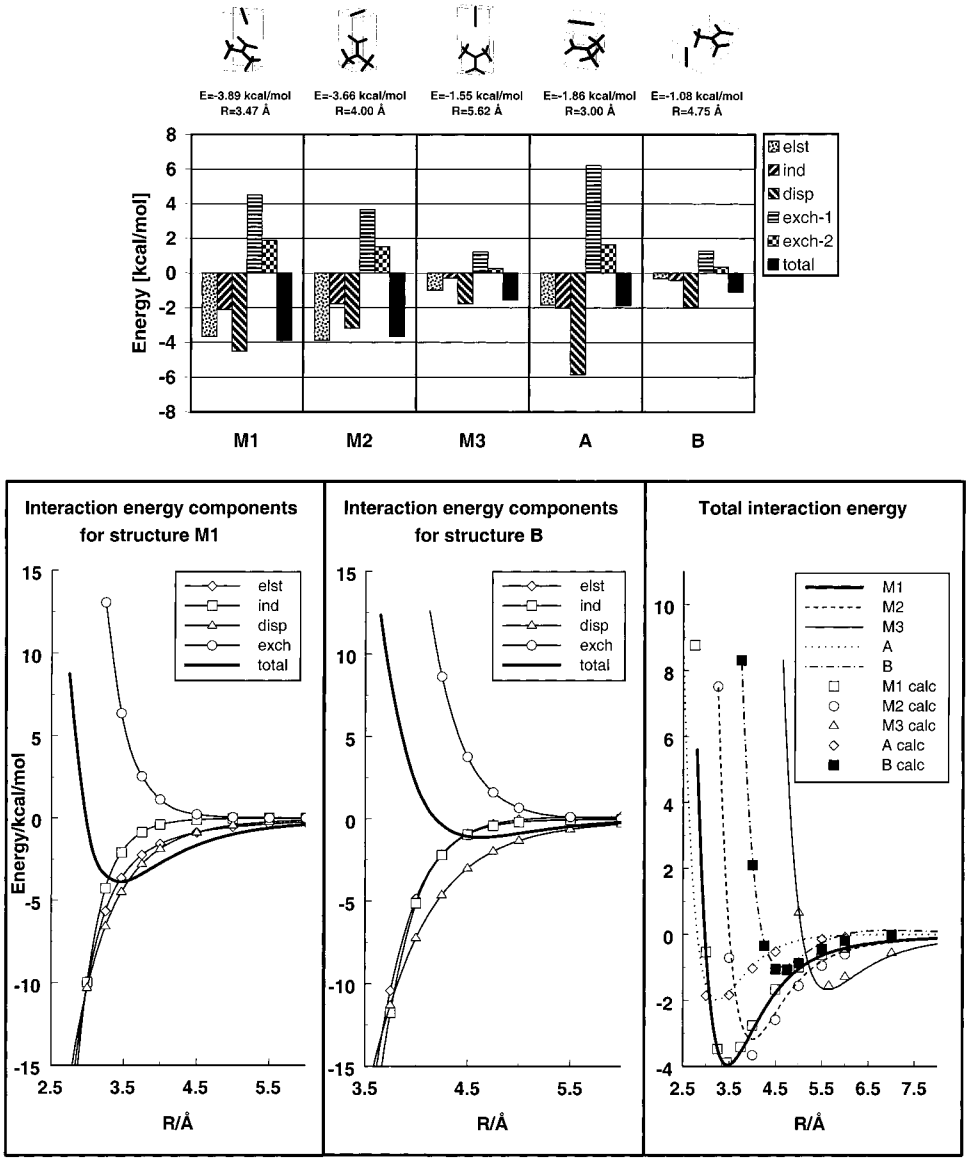

Figure 5. (a, top) Characteristic structures of the DMNA−CO_2 complex and decomposition of the corresponding interaction energies. Labels exch-1 and exch-2 denote the first- and second-order contributions to the exchange energy, calculated as $E^{(10)}_{exch}$ and $E^{(20)}_{exch-ind,resp} + E^{(20)}_{exch-disp} + \delta_{HF}$, respectively. (b, bottom) Radial dependence of the interaction energy components for various structures of the DMNA−CO_2 complex. See caption for Figure 2b.

system. This is clearly understood if one takes into account the large length of the CO_2 molecule and the presence of the voluminous methyl group in one of the monomers.

D. DMNA−CO_2 Complex. Parameters of the fit to the 289 energies (collected in Table S7) calculated at the LB level (eqs 12−15) are presented in Table S8. Three minimum structures M1, M2, and M3, obtained from the minimization of the potential energy are shown in Figure 5a along with two additional structures A and B (for parameters of the minima refer to Table 3).

A somewhat surprising asymmetric geometry of the global minimum M1 clearly results from a delicate balance between all the fundamental interaction energy components of similar magnitudes. The histogram shows that the most important binding factor in M1 is the dispersion energy followed by a slightly smaller electrostatic interaction. The stability of the structure M1 arises primarily from the competing tendencies to maintain a favorable dipole−quadrupole orientation and an orientation that maximizes dispersion interaction between oxygen atoms in CO_2 and the polarizable NO_2 group of DMNA. Thus, simple electrostatic arguments are not sufficient to predict the proper geometry of the global minimum. The tendency to favor the low-energy dipole−quadrupole orientation takes precedence in the minimum M2, where the roles of electrostatics and dispersion are reversed. Otherwise, proportions of all the components are very similar to those of M1 with somewhat smaller absolute values, so that the total interaction effect is only slightly less attractive than in M1. Although the geometry of the minimum M3 corresponds to the most optimal dipole−quadrupole orientation, the binding energy here is much smaller and the largest part of it is the dispersion interaction rather than electrostatics. The structure M3 is an interesting case of a fairly deep minimum at a very large center of mass separation, although, as we have seen before in a similar case, the nearest atom separation is not that large.

Structure A is an example of a dimer bound essentially by dispersion, which exceeds both electrostatics and induction by almost a factor of 3. The large first-order exchange energy, originating most probably from the interaction of one of the CO_2 oxygens with the nearby methyl groups, quenches a

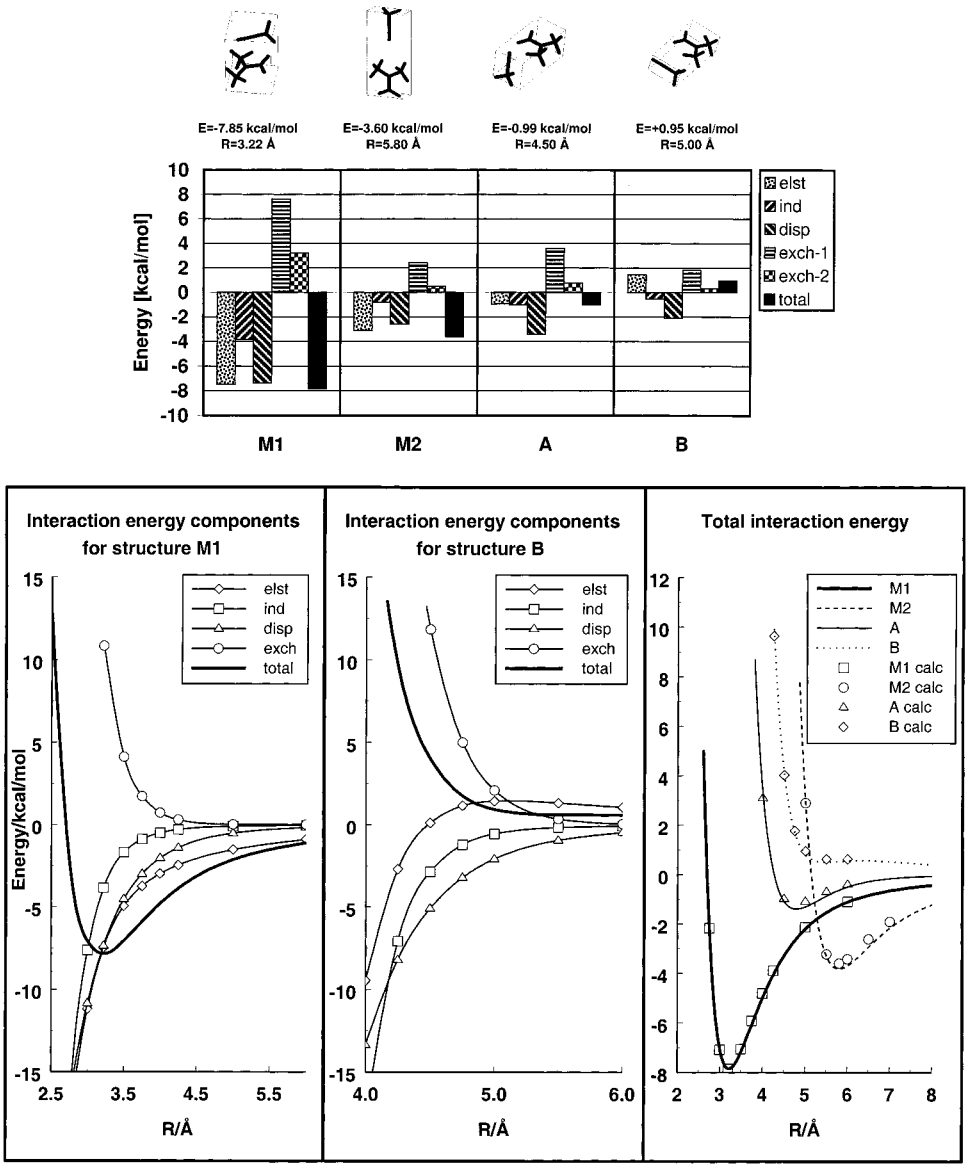

Figure 6. (a, top) Characteristic structures of the DMNA−CH_3CN complex and decomposition of the corresponding interaction energies. See caption for Figure 5a. (b, bottom) Radial dependence of the interaction energy components for various structures of the DMNA−CH_3CN complex. See caption for Figure 2a.

significant portion of the total attractive effect, leaving a relatively small binding energy of −1.54 kcal/mol (−1.86 kcal/mol as obtained directly from the SAPT calculation). The last histogram of Figure 5a shows that the structure B is yet another example of dispersion bound complex.

In Figure 5b the radial dependence of various interaction energy components and the total interaction energy are shown for various structures. It is seen that for configurations M1 and B the characteristic features of the energy decomposition are retained over a wide range of *R* separations. For example, the electrostatic and dispersion components for M1 are very similar not only in the minimum region, but also for other separations, and the induction energy never gets to dominate the interaction. On the other hand, for structure B the dispersion effect is responsible for most of the attractive interaction almost irrespective of *R*, while the electrostatics and induction energies are always much smaller and virtually identical.

The total interaction energies for all the configurations considered as obtained from the fit are plotted as functions of *R* in the last plot of Figure 5b along with the calculated values to help assess the fit quality. The radial minima for different angular configurations are scattered over a relatively wide range of *R*, reflecting high anisotropy of the system. It is interesting to note that although the monomers in configuration A experience a much less attractive effect than in the global minimum M1, they can approach each other much closer. On the other hand, the exchange repulsion between the CO_2 molecule and the methyl groups in configuration B keeps the monomers quite far apart and makes B the least attractive of all the configurations considered.

E. DMNA−CH_3CN Complex. Interaction energies calculated for this system at the LB level of SAPT, defined by eqs 12−15, for 504 configurations are collected in Table S9 and have been fitted using formula 20 with all the interaction sites coinciding with atoms. Parameters of this fit are presented in Table S10. Unconstrained minimization of the fitted potential energy led to two minimum structures M1 and M2 shown in Figure 6a. Parameters of these structures are also summarized in Table 3. From Figure 6a it is clear that both M1 and M2 correspond to favorable orientations of molecular dipoles and therefore the electrostatic energy is expected to provide most of the binding effect here. Decomposition of the interaction

energy presented in the histograms shows that the role of electrostatic interaction is indeed very large, but an almost equal amount of binding effect comes from the dispersion interaction. Clearly, the role of dispersion force increases with the size of monomers, as expected. The effect of induction is smaller but still nonnegligible. It is remarkable that the geometry M2, featuring the most favorable orientation of dipoles is *not* the global minimum, mostly due to the exchange energy which prevents the monomers from approaching each other closer and taking full advantage of the dipole arrangement. Instead, at shorter distances R, the interplay between all the fundamental interaction energy components leads to the slipped-antiparallel configuration M1. Although in this configuration the dipole−dipole alignment is less favorable than in M2, the binding energy, equal to −7.85 kcal/mol, is more than twice as large as in M2. It is also interesting to note that both for M1 and M2 most of the attractive contribution from electrostatics is canceled by the first-order exchange, so one may view the strong binding effect as mostly due to the corrections of the second order in V.

Structures A and B, also shown in Figure 6a, which do not correspond to local minima, feature two other orientations of dipoles. For structure A this orientation is neutral, which is reflected in a small electrostatic contribution. Most of the small binding effect for this structure comes from the dispersion interaction. For configuration B the electrostatic repulsion originating from parallel orientation of dipoles, along with the first-order exchange repulsion, overrides the attractive dispersion effect and give rise to a slightly positive total interaction energy. Figure 6b presents the radial dependence of the four fundamental components of the interaction energy for structures M1 and B, and of the total interaction energy for all structures considered. It is seen that for both M1 and B the hierarchy of various components depicted in the histograms of Figure 6a remains the same over a wide range of intermonomer separations. The induction interaction provides the smallest portion of the binding effect in both cases. The dispersion energy in M1 is in general close to electrostatics, although the latter has to dominate in the long range. It is interesting to note that due to the competition between repulsive dipole−dipole interaction and attractive higher multipoles interactions for $R = 4.5$ Å the repulsive electrostatic curve of structure B crosses zero and becomes attractive, so that for shorter distances the repulsion is purely of exchange origin. The radial cross sections through the potential energy surface shown in the last plot of Figure 6b have been generated from the fit and the calculated data points are also included for comparison. It is seen that the fit is doing quite a good job in reproducing the calculated energies, even those that were not included in the data set during the fitting process (all points for M1 and M2, and some points for A and B). The layout of the curves in the bottom plot of Figure 6b reflects quite a complicated landscape and a large anisotropy of the potential energy surface. While at the global minimum M1 the configurational space is penetrated down to $R = 3.23$ Å, other radial minima occur at significantly larger separations R. The very far position of the minimum M2 is somewhat misleading since for this semilinear configuration the separation of centers of mass does not really reflect the actual distances between the atoms of closest approach between the two monomers.

F. DMNA−CH_3OH Complex. The set of interaction energies computed at the LB level defined by eqs 12−15 for the 830 geometries collected in Table S11 has been used to fit the potential energy surface of this system. The optimized parameters are given in Table S12. Structural and energetic data for the DMNA−CH_3OH complex are collected in Table 3 and Figures 7, a and b. Figure 7a presents geometry and the interaction energy decomposition for two minimum structures M1 and M2, found by minimizing the fitted interaction energy, and two other structures, A and B, which do not correspond to local minima. The main binding factor for structures M1 and M2 is the electrostatic energy, attractive in both cases due to the favorable orientation of molecular dipoles. The peculiar nonsymmetric shape of M1 is an effect of competing tendencies to maintain the favorable dipole orientation and maximize the dispersion attraction between the hydroxyl and NO_2 groups while keeping the methyl groups of both monomers far apart to reduce the exchange repulsion. Indeed, from the histograms of Figure 7a it is seen that in M1 the electrostatic bonding effect is accompanied by a comparably strong dispersion interaction and an induction effect smaller by a factor of 2. Radial plot of Figure 7b confirms that these proportions of the four fundamental components of the interaction energy in configuration M1 are maintained for practically all intermolecular distances. Stability of the M2 structure, featuring the optimal dipole−dipole alignment, is dictated by electrostatics. The geometrical arrangement suggests the existence of a hydrogen bond between the hydroxyl group and an oxygen from the NO_2 group. A smaller role of dispersion in this configuration can be understood if one realizes that the distance between the polarizable oxygen atoms is larger than in M1. Configuration A differs from M2 roughly by 180° rotation of the CH_3OH molecule around its z axis. Such a rotation results in a highly repulsive dipoles orientation and breaking of the hydrogen bond, which leads to a repulsive potential energy curve. From Figure 7b one can see that the electrostatic component is repulsive except for regions of $R < 4.25$ Å, where the curve corresponding to this component crosses zero and the exchange repulsion starts to dominate the picture. The role of electrostatics as the factor determining the energetics of the complex is much smaller for configuration B. The orientation of dipoles in this structure is close to neutral and this fairly stable dimer is essentially dispersion bound.

Radial cross sections through the total interaction potential and comparison of the fit with the computed data are shown in the rightmost plot of Figure 7b. It is seen that the strongest bound configuration M1 is also the one with the smallest distance between the monomers. On the other hand, in the repulsive configuration A the monomers are kept apart by the repulsive wall starting already at $R \approx 4.0$ Å.

G. DMNA Dimer. In order to fit the potential energy surface of this system we used interaction energies calculated for 433 geometries in the dimer-centered basis set, at the SCF + $E_{\mathrm{disp}}^{(20)}$ level of theory. These geometries and the corresponding energies are presented in Table S13, while the fit parameters have been collected in Table S14. Minimum structures M1−M5 resulting from the minimization of the fitted potential along with one additional repulsive configuration A are shown in Figure 8a. Since the computational strategy applied to this system does not provide natural decomposition of the SCF interaction energy, additional single-point SAPT calculations have been performed for each of the above geometries to obtain the fundamental interaction energy components presented in the histograms.

From Figure 8a one can see that the induction contributions are generally small, and the electrostatics and first-order

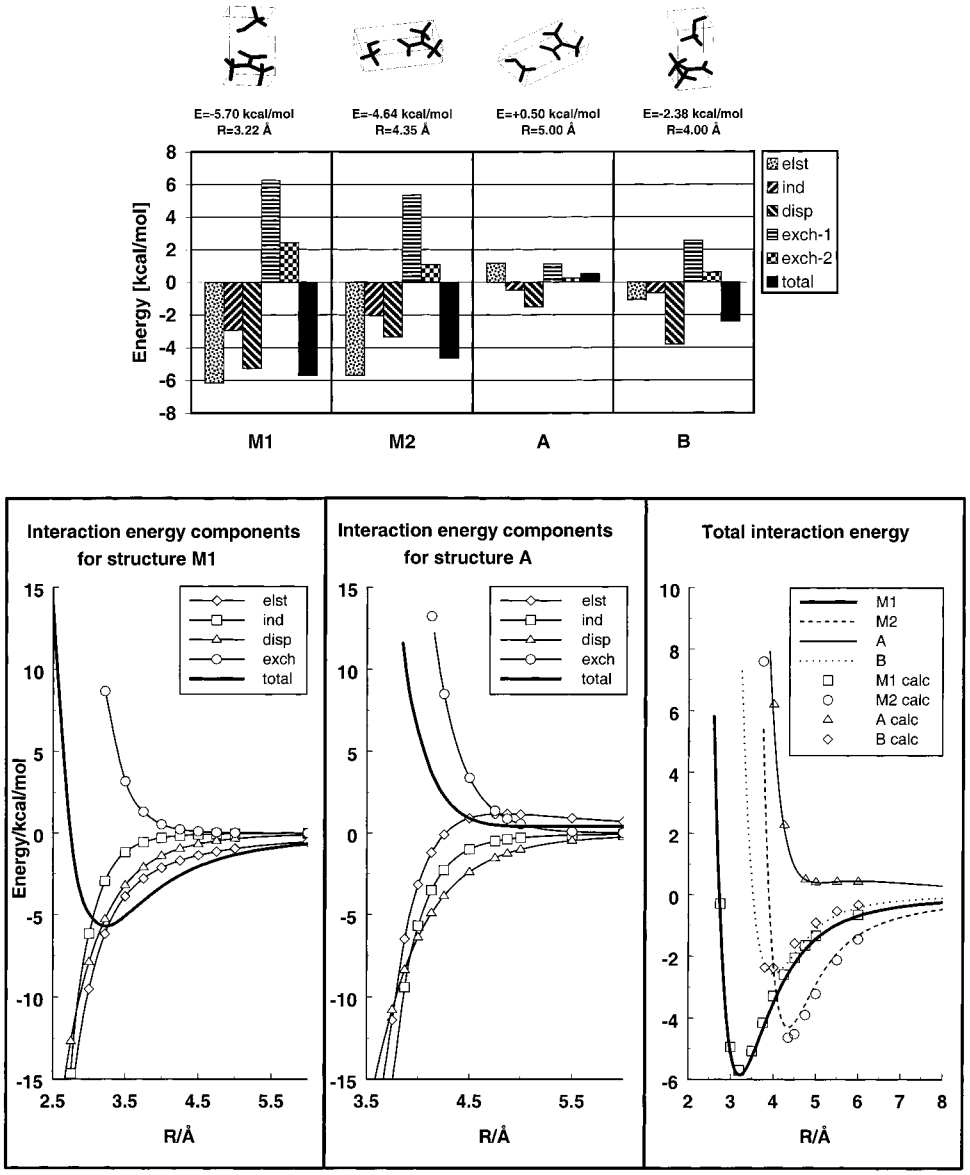

Figure 7. (a, top) Characteristic structures of the DMNA−CH_3OH complex and decomposition of the corresponding interaction energies. See caption for Figure 5a. (b, bottom) Radial dependence of the interaction energy components for various structures of the DMNA−CH_3OH complex. See caption for Figure 2b.

exchange are the main components of the supermolecular SCF interaction energy. This energy is positive for all the structures considered, including the M1 and M3 structures, corresponding to favorable orientations of molecular dipoles. In these structures the attractive contribution of the electrostatic energy is quenched by the first-order exchange effects and the dispersion turns out to be the major binding force. In the M5 complex, where the dipole−dipole orientation results in a repulsive electrostatic effect, dispersion is the dominating attractive component. Repulsive electrostatics determines the energetics of the configuration A. From Figure 8b it is seen that in spite of the significant dispersion contribution, the total interaction energy for this configuration is always positive. Radial cross sections through the total potential energy surface, shown in the last plot of Figure 8b, reveal the large anisotropy of the interaction, manifesting itself in the wide scatter of the radial minima locations. This feature seems to be natural for a dimer composed of spatially extended systems. The global minimum M1 is significantly distinct from the others: its depth is almost twice as large as that of the next minimum, and its position corresponds to a much shorter intermonomer distance. Thus, one can interpret the minimum structure as due to spatial orientation which favors the closest approach of monomers by minimizing the exchange repulsion. The close approach results in a large dispersion interaction since many electron pairs are near each other. Notice that this picture is very different from the traditional description of the interactions of large molecules which emphasizes the dipole−dipole forces. The other minima, although occurring over a wide range of R, exhibit well depths quite similar to one another.

VI. Accuracy Considerations

Due to the large size of the molecular systems involved and high dimensionality of the potential energy surfaces, the calculations presented in this work have been performed in basis sets of moderate size. Some insight into the quality of these bases can be obtained by assessing the accuracy of the calculated monomer properties. In Table 4 we present the leading multipole moments and dipole polarizability components calculated for each system at the MBPT2 level in the monomer part of the basis set. Where available, the corresponding experimental data

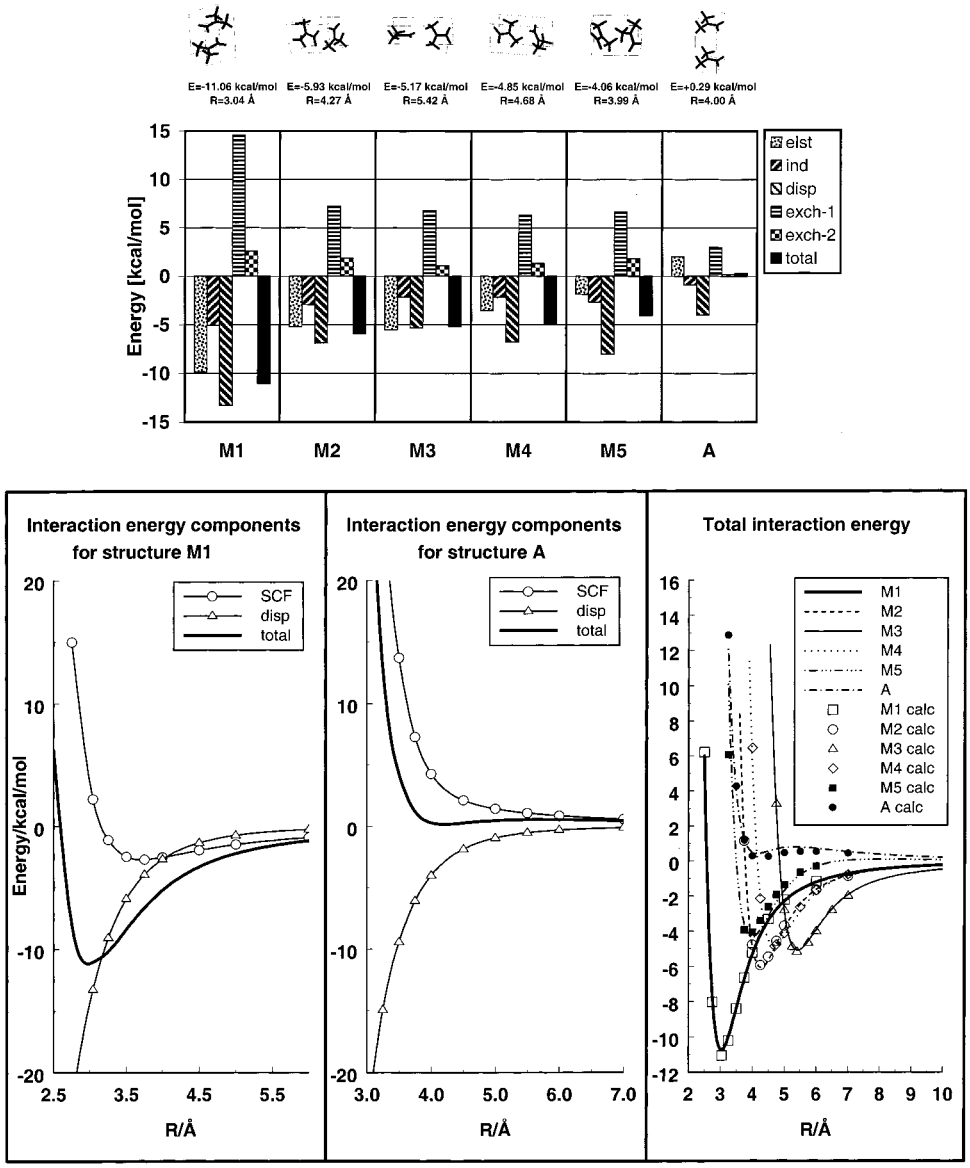

Figure 8. (a, top) Characteristic structures of the DMNA dimer and decomposition of the corresponding interaction energies. Labels exch-1 and exch-2 denote the first- and second-order contributions to the exchange energy, calculated as $E_{exch}^{(10)}$ and $E_{exch-ind,resp}^{(20)} + \delta_{HF}$, respectively. (b, bottom) Radial dependence of the interaction energy components for various structures of the DMNA dimer. See caption for Figure 2b.

are also given. It can be seen that, in spite of the moderate sizes of our basis sets, the multipole moments are reproduced fairly accurately, being within 10% of the experimental values. Although the polarizabilities are much more basis set demanding, even in this case the errors do not exceed 20%. These errors are further reduced during the calculation of the interaction energies, as the basis set describing a monomer contains then both the far-bond and mid-bond functions. It should be remembered also that the discrepancies observed in Table 4 are partly due to the truncation of the correlation treatment at the MBPT2 level and would be reduced upon extending the calculations to higher orders.

To examine the accuracy of our potential energy surfaces in more detail, additional SAPT calculations have been performed for the minimum structures of the $(CH_3CN)_2$, $(CH_3OH)_2$, and CH_3OH-CO_2 complexes at the LA level of theory, using an extended 5s3p2d1f/3s2p basis set composed of contracted Partridge orbitals in the isotropic parts, and the interaction-energy optimized polarization functions. This basis, described in detail in ref 6, is expected to provide results accurate up to 0.1 kcal/mol.[6] It turned out that for the M1 minimum of the

TABLE 4: Leading Multipole Moments (at the MBPT2 Level Including Orbital Relaxation) and Polarizabilities (at the RPA+MBPT2 Level) of the Monomers Calculated in This Work in the Monomer Basis Sets (All Quantities in Atomic Units)

			CH_3OH		CO_2	
	DMNA 3s2p1d	CH_3CN 3s2p1d	3s2p1d	4s2p1d	3s2p1d	4s2p1d
μ	−1.373	1.431	0.595	0.622		
		1.54[a]	0.665[b]			
Q_{zz}					−2.723	−2.901
					−3.19[c]	
α_{zz}	60.725	34.070	20.398	21.112	25.863	27.365
		40.90[d]			26.71[e]	
α_{xx}	58.723	21.020	18.159	18.774	10.425	11.321
		25.17[d]			12.91[e]	
α_{yy}	35.703	21.020	16.975	17.687	10.425	11.321
α_{xz}			1.029	0.930		

[a] Experimental value from ref 34. [b] Experimental value from ref 28. [c] Reference 35, from birefringence measurements. [d] From anisotropy and mean polarizability data of ref 36. [e] From experimental anisotropy and mean polarizability data of ref 37.

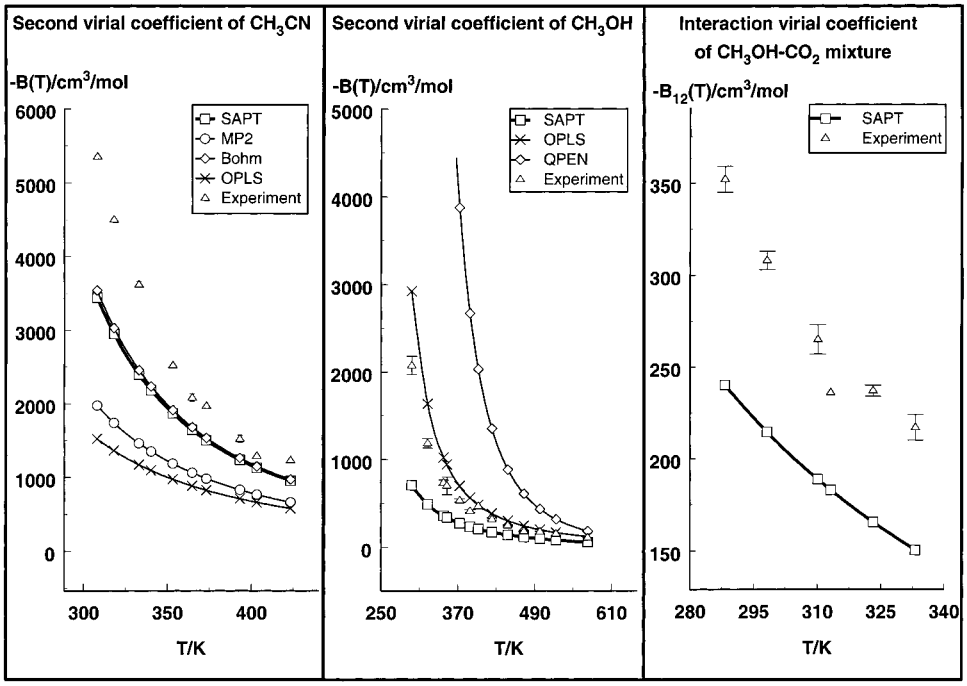

Figure 9. Second virial coefficients for CH_3CN, CH_3OH, and the CH_3OH-CO_2 mixture. Experimental data from ref 38. Literature potentials: MP2, ref 9; Böhm, ref 11; OPLS, ref 10 for CH_3CN and ref 13 for CH_3OH; QPEN, ref 16.

CH_3CN dimer this large basis gave the interaction energy by 0.53 kcal/mol lower than our regular basis. For the M1, S, and M2 structures of the CH_3OH dimer the large basis results were lower by 0.3, 0.43, and 0.32 kcal/mol, respectively, from the ones computed in smaller bases. For the CH_3OH-CO_2 complex the large-basis energy of the M3 structure came out 0.11 kcal/mol higher, while the M1 and M2 structures experienced an additional stabilization of about 0.25 kcal/mol. In all cases the largest attractive contribution to the observed basis set effects resulted from the leading dispersion term, $E_{disp}^{(20)}$. This contribution was enhanced or quenched by the contribution from the electrostatic energy, $E_{elst}^{(10)}$, which assumed different signs, depending on the structure considered. Basis-set dependence of the other corrections, especially the intramonomer correlation ones, turned out to be much less important.

Large basis set results for the CH_3CN dimer can be used to estimate the accuracy of the interaction energies of systems involving DMNA, which have been calculated in the same small basis set. Here, besides the basis set incompleteness error, we also have to take into account the truncation of theory level. The basis set effect on the LB level interaction energies in all complexes involving DMNA can be roughly estimated if the relative basis set unsaturation errors of the E_{int}^{HF} and $E_{disp}^{(20)}$ components are assumed to be the same as for the CH_3CN dimer in the M1 configuration (5% and 8%, respectively). Further, assuming that the ratios of the intramonomer correlation contributions in the electrostatic, induction, dispersion, and exchange energies to their uncorrelated counterparts are approximately system-independent and equal to those in the CH_3CN dimer, one can come up with an estimate of the neglected intramonomer correlation effects. For all the characteristic structures of the complexes considered except for $(DMNA)_2$ this procedure yielded the error bars not exceeding 0.7 kcal/mol. In the case of the DMNA dimer the error estimate must also include the exchange-dispersion correction, $E_{exch-disp}^{(20)}$, not present in the calculations for this complex. Assuming this correction to be approximately equal to 10% of the absolute value of $E_{disp}^{(20)}$ and estimating the remaining errors as for other systems involving DMNA, we conclude that the calculated minima M1−M5 are accurate up to at least 1 kcal/mol and slightly too deep. It should be noted that the error introduced by neglecting the positive exchange correction $E_{exch}^{(20)}$ cancels to a large extent the basis set incompleteness error of $E_{disp}^{(20)}$.

As one more check on the accuracy of the calculated potential energy surfaces, we calculated the second virial coefficients $B(T)$ for acetonitrile and methanol, and the interaction second virial coefficient $B_{12}(T)$ for the CH_3OH-CO_2 mixture. The results of these calculations are presented in Figure 9 along with the corresponding experimental data[38] and the data obtained from other potential functions. It is seen that for all systems and all temperatures considered the coefficients calculated from the SAPT potential are smaller in absolute value than their experimental counterparts. This is clearly the result of insufficient depth of the potential wells, a consequence of the unsaturated dispersion component of the interaction energy. This factor is probably also responsible for poor values of $B(T)$ generated for CH_3CN dimer from the MP2 potential of ref 9. It is interesting to note that for this system the SAPT values of $B(T)$ are virtually identical to the ones derived from the empirical potential of Bohm et al.[11] which are closest to experimental data. The curve corresponding to the OPLS potential of Jorgensen and Briggs[10] lies significantly below the experimental points, indicating that the potential well is too shallow. In the case of the CH_3OH dimer, the OPLS potential of Jorgensen[13] gives the second virial coefficients in best agreement with experiment. The curve corresponding to the SAPT potential is slightly below, indicating underestimation of the interaction energy. In the QPEN potential, on the other hand, the interaction is largely overestimated, which manifests itself in too high absolute values of $B(T)$. As expected, the relative location of $B(T)$ curves corresponding to different potentials correlates well with the energetic sequence of the predicted global minima. Potential functions with deeper minima give more negative values of the second virial coefficient.

VII. Summary and Conclusions

Symmetry-adapted perturbation theory has been employed to generate seven *ab initio* interaction potential energy surfaces for the complexes $(CH_3CN)_2$, $(CH_3OH)_2$, CH_3OH-CO_2, DMNA$-CO_2$, DMNA$-CH_3CN$, DMNA$-CH_3OH$, and $(DMNA)_2$. The calculations have been performed in spd basis sets containing bond functions. For complexes not involving the DMNA molecule, the highest available level of SAPT has been applied, while the remaining systems were treated in a more approximate manner. High-level large-basis-set calculations for selected geometries allow to estimate that the error of the computed interaction energies at minimum structures should not exceed 1 kcal/mol for the DMNA dimer and 0.7 kcal/mol for the other systems. Comparison of the calculated second virial coefficients for CH_3CN, CH_3OH, and CH_3OH-CO_2 mixture with experimental data indicates that the predicted potential depths are generally too small, an inevitable consequence of a moderate basis set size. Nevertheless, in the case of the SAPT potentials the agreement with experiment is usually better than for other potentials, including the empirically derived ones.

The multipole moments as well as the induction and dispersion asymptotic coefficients have been computed for all systems at levels consistent with the short-range SAPT calculations. This information about the asymptotic behavior of the interaction energy has been then utilized to obtain charges and long-range coefficients of the site−site fits to the calculated energy data. In this way the proper asymptotic behavior of the fits has been assured.

A common feature of all the potential energy surfaces considered is their large anisotropy resulting from the spatial extent of the interacting molecules. Analysis of the fits allows to determine the minima on the potential energy surfaces, whereas the decomposition of the interaction energy inherent to the SAPT theory provides physical insight into the nature of the interactions. For all complexes considered the geometry of energetically favored structures results from an interplay between electrostatic, dispersion, induction, and exchange interactions, and none of them can be neglected when considering the shape and stability of a complex. Due to relatively large dipole moments, and a large quadrupole moment in the case of CO_2, the electrostatic interaction usually plays an important role in determining the structures. However, simple electrostatic arguments often lead to incorrect conclusions about the energetic sequence of the predicted minima, and sometimes the existence of a minimum cannot be explained at all using these arguments. In most cases the electrostatic interaction is accompanied by a dispersion contribution of a comparable size. This contribution is not only responsible for a large fraction of the interaction energy. The trend to maximize the dispersion interaction plays also an important role in determining the shape of the complex. The induction effects are generally smaller than the other corrections, but sometimes they may become as large as dispersion.

The observations made above challenge the established methods of analyzing interactions of large molecules, in particular molecules of biological interest. The current paradigm is that the minimum structures can be well described by considering only the interactions of the multipole moments of such molecules. This subject has been the area of active research and advanced methods of calculating multipolar interactions for large molecules have been developed (see, e.g., refs 39−42). If the observations from this work extend to other systems, considerations based on the electrostatic interaction alone cannot be trusted as a reliable tool in analysis of the interactions of large molecules. Although in the minima the electrostatics often seems to provide quite a good approximation to the total interaction energy due to cancellations between the other components, the latter cannot be neglected if the correct configurations of these minima are to be determined. The preferred configurations will be dictated not only by the electrostatic interaction but also by geometric factors related to the exchange effects (valence shell repulsion). Minimization of these effects will usually distort the favorable orientation of molecular multipoles, but at the same time will allow closer approach of the two monomers resulting in a large attractive dispersion interaction.

Out of the two cosolvents considered, the CH_3CN molecule exhibits the largest affinity toward the DMNA molecule. The DMNA$-CH_3CN$ binding energy of 7.9 kcal/mol is 2 kcal/mol larger than that of the DMNA$-CH_3OH$ complex, and 4 kcal/mol larger than the DMNA$-CO_2$ interaction. Due to the large electrostatic and dispersion forces, the DMNA dimer experiences the largest binding effect of all the complexes considered in this work. In the deepest minimum of this complex (M1) the calculated interaction energy is equal to −11.1 kcal/mol.

When combined with the previously calculated SAPT potentials for the CO_2 dimer[6] and the CH_3CN-CO_2 complex,[7] the new set of potential energy surfaces is sufficient for a fully *ab initio* Monte Carlo and/or molecular dynamics simulations of the processes occurring in solutions of DMNA in supercritical CO_2 in the presence of CH_3CN or CH_3OH as cosolvents. However, one has to realize that the SAPT potentials are strictly two-body potentials and do not include three-body and higher nonadditive effects. Such effects have to be included in simulations for polar molecules.[43] Rigorous *ab initio* description of nonadditive effects for molecules of the size considered in this paper is beyond present-day computational capabilities. Fortunately, these effects are well approximated by the simple asymptotic induction nonadditivity model.[43] The multipole moments and polarizabilities used to build this model are given in Table 4. When applying this model with SAPT two-body potentials one has to remember not to double count the two-body induction effects, already included in the potential developed here.

Acknowledgment. This work was supported by the Strategic Environmental Research and Development Program (SERDP), Project PP-695. The authors gratefully acknowledge the computer resources made available for this study on SGI Power Challenge Array and Origin 2000 Array by the DOD High Performance Computing Site at the Army Research Laboratory, Aberdeen Proving Ground, MD. Partial support by the NSF Grant CHE-9626739 is gratefully acknowledged. We thank Dr. Joanna Sadlej for performing the pilot calculations for the DMNA$-CO_2$ complex, and Professor Bogumił Jeziorski for valuable discussions.

Supporting Information Available: Tables S1, S3, ..., S13 contain the grid data and all the SAPT interaction energy components computed for each system. The parameters of the fits to the potential energy surfaces are presented in Tables S2, S4, ..., S14. This material is available free of charge via the Internet at http://pubs.acs.org.

References and Notes

(1) Chałasiński, G.; Szczęśniak, M. M. *Chem. Rev.* **1994**, *94*, 1723.

(2) Jeziorski, B.; Moszyński, R.; Szalewicz, K. *Chem. Rev.* **1994**, *94*, 1887.

(3) Szalewicz, K.; Jeziorski, B. In *Molecular Interactions—From van der Waals to Strongly Bound Complexes*; Scheiner, S., Ed.; Wiley: New York, 1997; p 3.

(4) Jeziorski, B.; Szalewicz, K. Intermolecular Interactions by Perturbation Theory. In *Encyclopedia of Computational Chemistry*; von Ragué Schleyer, P., et al., Eds.; Wiley: New York, 1998.

(5) Schroeder, M. A.; Fifer, R. A.; Morris, J. B. *The Relationship of Chemical Structure to Supercritical-Fluid Solubility and to Cosolvent-Modifier Properties: A Literature Review*; ARL Report, June 1995.

(6) Bukowski, R.; Sadlej, J.; Jeziorski, B.; Jankowski, P.; Szalewicz, K.; Kucharski, S. A.; Williams, H. L.; Rice, B. M. *J. Chem. Phys.* **1998**, *110*, 3785.

(7) Williams, H. L.; Rice, B. M.; Chabalowski, C. F. *J. Phys. Chem. A* **1998**, *102*, 6981.

(8) Edwards, H. J.; Madden, P. A.; McDonald, I. R. *Mol. Phys.* **1984**, *51*, 1141.

(9) Cabaleiro-Lago, E. M.; Ríos, M. A. *J. Phys. Chem. A* **1997**, *101*, 8327.

(10) Jorgensen, W. L.; Briggs, J. M. *Mol. Phys.* **1988**, *63*, 547.

(11) Böhm, H. J.; McDonald, I. R.; Madden, P. A. *Mol. Phys.* **1983**, *49*, 347. Böhm, H. J.; Ahlrichs, R.; Scharf, P.; Schiffer, H. *J. Chem. Phys.* **1984**, *81*, 1389.

(12) Popelier, P. A. L.; Stone, A. J.; Wales, D. J. *Faraday Discuss.* **1994**, *97*, 243.

(13) Jorgensen, W. L. *J. Phys. Chem.* **1986**, *90*, 1276.

(14) Pálinkás, G.; Hawlicka, E.; Heinzinger, K. *J. Phys. Chem.* **1987**, *91*, 4334.

(15) Snir, J.; Nemenhoff, R. A.; Scheraga, H. A. *J. Phys. Chem.* **1978**, *82*, 2497.

(16) Marchese, F. T.; Mehrotra, P. K.; Beveridge, D. L. *J. Phys. Chem.* **1982**, *86*, 2592.

(17) Jeziorski, B.; Moszynski, R.; Ratkiewicz, A.; Rybak, S.; Szalewicz, K.; Williams, H. L. In *Methods and Techniques in Computational Chemistry: METECC94, Vol. B Medium-Size Systems*; Clementi, E., Ed.; STEF: Cagliari, Italy, 1993; p 79.

(18) Rybak, S.; Jeziorski, B.; Szalewicz, K. *J. Chem. Phys.* **1991**, *95*, 6576.

(19) Cwiok, T.; Jeziorski, B.; Kołos, W.; Moszynski, R.; Szalewicz, K. *J. Mol. Struct. (Theochem.)* **1994**, *307*, 135.

(20) Brink, C. M.; Satchler, G. R. *Angular Momentum*; Clarendon: Oxford, UK, 1975.

(21) Wormer, P. E. S. Ph.D. Thesis, Nijmegen, 1975.

(22) van der Avoird, A.; Wormer, P. E. S.; Mulder, F.; Berns, R. M. *Top. Curr. Chem.* **1980**, *93*, 1.

(23) Wormer, P. E. S.; Hettema, H. *J. Chem. Phys.* **1992**, *97*, 5592. *POLCOR* package, University of Nijmegen, 1992.

(24) Mas, E. M.; Szalewicz, K.; Bukowski, R.; Jeziorski, B. *J. Chem. Phys.* **1997**, *107*, 4207.

(25) Tang, K. T.; Toennies, J. P. *J. Chem. Phys.* **1984**, *80*, 3726.

(26) Mas, E. M.; Szalewicz, K. *J. Chem. Phys.* **1996**, *104*, 7676.

(27) Granar, G.; Rossetti, C.; Bailly, D. *Mol. Phys.* **1986**, *58*, 627. Granar, G. In *Accurate Molecular Structure*; Domenicano, A., Hatgittai, I., Eds.; Oxford University Press: London, 1992; p 65.

(28) Moruzzi, G.; Winnewisser, B. P.; Winnewisser, M.; Mukhopadhyay, I.; Strumia, F. *Microwave, Infrared, and Laser Transitions of Methanol. Atlas of Assigned Lines from 0 to 1258 cm*$^{-1}$; CRC Press: New York, 1995.

(29) Stolevik, R.; Rademacher, P. *Acta Phys. Scand.* **1969**, *23*, 672.

(30) Dunning, T. H., Jr. *J. Chem. Phys.* **1989**, *90*, 1007.

(31) Williams, H. L.; Mas, E. M.; Szalewicz, K.; Jeziorski, B. *J. Chem. Phys.* **1995**, *103*, 7374.

(32) Partridge, H. *J. Chem. Phys.* **1987**, *87*, 6643; *90*, 1043. NASA Technical Memorandum 89449, 101044, 103918. Partridge, H.; Faegri, K., Jr. *Theor. Chim. Acta* **1992**, *82*, 207.

(33) Moszynski, R.; Cybulski, S. M.; Chalasinski, G. *J. Chem. Phys.* **1994**, *100*, 4998.

(34) West, R. C., Ed. *CRC Handbook of Chemistry and Physics*, 64th ed.; CRC Press, Inc.: Boca Raton, FL, 1984.

(35) Watson, J. N.; Craven, I. E.; Ritchie, G. L. D. *Chem. Phys. Lett.* **1997**, *274*, 1.

(36) Gray, C. G.; Gubbins, K. E. *Theory of Molecular Fluids*; Oxford University Press: Oxford, UK, 1984; Vol. 1.

(37) Cai, W. Q.; Gough, T. E.; Gu, X. J.; Isenor, N. R.; Scoles, G. *Phys. Rev. A* **1987**, *36*, 4722.

(38) Dymond, J. H.; Smith, E. B. *The Virial Coefficients of Pure Gases and Mixtures*; Oxford University: London, 1980.

(39) Dykstra, C. E. *Chem. Rev.* **1993**, *93*, 2339.

(40) Stone, A. J. *The Theory of Intermolecular Forces*; Clarendon: Oxford, UK, 1996.

(41) Sokalski, W. A.; Sawaryn, A. *J. Mol. Struct. (Theochem)* **1992**, *88*, 91.

(42) Strasburger, K. *Comput. Chem.* **1994**, *22*, 7.

(43) Mas, E. M.; Bukowski, R.; Szalewicz, K. *J. Chem. Phys.*, to be published.